References

Abramowitz, M., Stegun, A., 1970. Handbook of Mathematical Functions, Section 3.9.7. Dover Publications Inc.

Altiparmakov, D. V., Tomašević, D. I., 1990. Variational Formulation of a Higher Order Nodal Diffusion Method. Nucl. Sci. Eng. 105 (3), 256–270.

An, T., Owen, A. B., 2001. Quasi-Regression. Journal of Complexity 17 (4), 588 – 607.

Antonopoulous, P., 1972. Large Mesh Model Development Study. Ph.D. thesis, Mass. Inst. Tech., Cambridge, M.A.

Bahadir, T., Lindahl, S. O., 2006. SIMULATE-4 Pin Power Calculations. PHYSOR-2006, ANS Topical Meeting on Reactor Physics, Vancouver, Canada.

Bahadir, T., Lindahl, S. O., 2009. Studsviks Next Generation Nodal Code SIMULATE-5. Advances in Nuclear Fuel Management IV (ANFM 2009).

Bahadir, T., Lindahl, S. O., Palmtag, S. P., 2005. SIMULATE-4 Multigroup Nodal Code with Microscopic Depletion Model. ANS Topical Meeting in Mathematics and Computations, Avignon, France.

Ball, G., 1999. Efficient Use of Neutrons at SAFARI-1. In: Trans. Intl. Conf. Research Reactor Fuel Management (RRFM'99), March 29-31. Bruges, Belgium.

Beam, T. M., Ivanov, K. N., Baratta, A. J., Finnemann, H., 1999. Nodal Kinetics Model Upgrade in the Penn State Coupled TRAC/NEM Codes. Annals of Nuclear Energy 26, 1205–1219.

Bennewitz, F., Finnemann, H., Wagner, M. R., 1975. Higher-order Corrections in Nodal Reactor Calculations. Trans. Am. Nucl. Soc. 22, 250.

Boer, R., Finnemann, H., 1992. Fast Analytical Flux Reconstruction Method for Nodal Space-time Nuclear Reactor Analysis. Annals of Nuclear Energy 19 (10-12), 617–628.

Brown, F. B., Barrett, R. F., Booth, T. E., Bull, J. S., 2002. MCNP version 5. Trans. Am. Nucl. Soc. 87, 273 – 276.

Chao, Y. A., 1995. Unifying via Conformal Mapping Coarse-mesh Neutron Diffusion Calculations in Cartesian and Hexagonal Geometries. Journal of Computational and Applied Mathematics 63, 449.

Cho, N. Z., 2006. The AFEN Method in Cylindrical Geometry for Pebble Bed Reactors - Extension to Multigroup Form and Treatment of Voids. Trans. Am. Nucl. Soc. 94, 553.

Cho, N. Z., Kim, Y. H., Park, K. W., 1997. Extension of Analytic Function Expansion Nodal Method to Multi-group Problems in Hexagonal-Z Geometry. Nucl. Sci. Eng. 126, 35.

Department of Energy, 2011. Integrated Resource Plan for Electricity in South Africa 2010 - 2030.

Dilbert, I., Lewis, E. E., 1985. Variational nodal methods for Neutron Transport. Nucl. Sci. Eng. 91, 132 – 142.

Dorning, J. J., 1979. Modern Coarse Mesh Methods, A Development of the 70s. Proc. Conf. Computational Methods in Nuclear Engineering, Williamsburgh, VA., US Department of Energy, 1–3.

Downar, T., Lee, D., Xu, Y., Kozlowski, T., 2004. Theory Manual for the PARCS Neutronic Core Simulator. Tech. rep., Purdue University.

Duderstadt, J., Hamilton, L., 1976. Nuclear Reactor Analysis. John Wiley & Sons, New York.

Finnemann, H., Bennewitz, F., Wagner, M. R., 1977. Interface Current Techniques for Multidimensional Reactor Calculations. Atomkernenergie 30 (2), 123–128.

Finnemann, H., Boer, R., Muller, R., 1992. Combination of Finite-difference and Finite-volume Techniques in Global Reactor Calculations. Kerntechnik 57(4), 216 – 222.

Froehlich, R., 1972. Flux Synthesis Methods versus Difference Approximation Methods of Neutron Flux Distributions in Fast and Thermal Reactors. Tech. rep., IAEA, Vienna.

Golfier, H., Lenain, R., Calvin, C., Lautard, J. J., Baudron, A. M., Fougeras, P., Magat, P., Martinolli, E., Dutheillet, Y., 2009. Apollo3: a common project of CEA, AREVA and EDF for the Development of a new Deterministic Multi-purpose Code for Core Physics Analysis. International Conference on Mathematics, Computational Methods & Reactor Physics, Saratoga Springs.

Greenspan, H., Kelber, C. N., Okrent, D., 1968. Computational Methods in Reactor Physics. Gordon and Breach, New York.

Griebel, M., Grestner, T., 1998. Numerical Integration using Sparse-grids. Numerical Algorithms 18, 209–232.

Grossman, L., Hennart, J.-P., 2007. Nodal Diffusion Methods for Space-time Neutron Kinetics. Progress in Nuclear Energy 49, 181–216.

Guessous, N., Akhmouch, M., 2002. Higher Order Analytical Nodal Methods in Response-matrix Formulation for the Multigroup Neutron Diffusion Equations. Annals of Nuclear Energy 29 (15), 1765–1778.

Gupta, N., 1981. Nodal Methods for Three-dimensional Simulators. Progress in Nuclear Energy 7, 127–149.

Hendriks, J. A., 2006. Neutronics Validation during Conversion to LEU. In: Proceedings of PHYSOR 2006, September 10 - 14. Vancouver, BC, Canada.

Joo, H. G., Yoon, J. I., Baek, S. G., 2009. Multigroup Pin Power Reconstruction with Two-Dimensional Source Expansion and Corner Flux Discontinuity. Annals of Nuclear Energy 36 (1), 85–97.

Kang, C., Hansen, K. F., 1973. Finite Element Methods for Reactor Analysis. Nucl. Sci. Eng. 51, 456–495.

Koebke, K., Hetzelt, L., 1985. On the Reconstruction of Local Homogeneous Neutron Flux and Current Distributions of Light Water Reactors from Nodal Schemes. Nucl. Sci. Eng. 91 (2), 123–131.

Koebke, K., Wagner, M. R., 1977. The Determination of the Pin Power Distribution in a Reactor Core on the Basis of Nodal Coarse Mesh Calculations. Atomkernenergie 30, 136.

Langenbuch, S., Maurer, W., Werner, W., 1977a. Coarse-mesh Flux Expansion for the Analysis of Space-time Effects in Large Light Water Reactor Cores. Nucl. Sci. Eng. 63, 437–456.

Langenbuch, S., Maurer, W., Werner, W., 1977b. High-order Schemes for Neutron Kinetics Calculations, based on Local Polynomial Approximation. Nucl. Sci. Eng. 64, 508–516.

Lautard, J. J., Loubiere, S., Fedon-Magnaud, C., 1991. Three-dimensional Pin-by-pin Core Diffusion Calculation. In: Proceedings of the International topical meeting on Advances in mathematics, computations and reactor physics. Pittsburgh, USA.

Lawrence, R., Dorning, J., 1980. A nodal Greens Function method for Multidimensional Neutron Diffusion Calculations. Nucl. Sci. Eng. 76, 218–231.

Lawrence, R. D., 1986. Progress in Nodal Methods for the Solution of the Neutron Diffusion and Transport Equations. Progress in Nuclear Energy 17 (3), 271–301.

Lee, R. R., 1977. Argonne Code Centre: Benchmark Problem Book, ANL-7416, Suppl. 2. Tech. rep., ANL.

Leege, P. F. A. D., Reitsma, F., 2001. HOR : Criticality Comparison Using a Nodal Code , Monte Carlo Codes and Plant Data. In: Proceedings of International Conference on Mathematics Computational Methods and Reactor Physics (M&C 2001)., September. Salt Lake City, Utah, USA.

Lefebvre, J. C., Mondo, J., West, J., 1991. Benchmark Calculations of Power Distributions within Assemblies, NEACRP-L-336. Tech. rep., NEA.

Lemieux, C., Owen, A. B., 2002. Quasi-regression and the Relative Importance of the ANOVA Components of a Function in Monte Carlo and quasi-Monti Carlo Methods. Springer-Verlag, Berlin.

Leppanen, J., 2007. Development of a New Monte Carlo Reactor Physics Code. Ph.D. thesis, Helsinki University of Technology.
URL `http://montecarlo.vtt.fi/download/P640.pdf`

Lewis, E. E., 2001. Benchmark Specification for Deterministic 2D/3D MOX Fuel Assembly Transport Calculation without Spatial Homogenization (C5G7 MOX). Tech. rep., NEA/NSC/DOC.

Lozano, J., 2007. Development and Performance of the Analytic Nodal Diffusion SolverANDES'in Multigroups for 3D Rectangular Geometry. Joint International Topical Meeting on Mathematics & Computation and Supercomputing in Nuclear Applications (M&C+ SNA 2007).

Makai, M., 1984. Response Matrix of Symmetric Nodes. Nucl. Sci. Eng. 86, 302.

Marleau, G., Roy, R., Hébert, A., 1994. DRAGON: A Collision Probability Transport Code for Cell and Supercell Calculations. Report IGE–157, Institut de genie nucleaire, Ecole Polytechnique de Montreal, Montreal, Quebec.

Muller, E., Weiss, Z. J., 1991. Benchmarking with the Multigroup Diffusion High-order Response Matrix Method. Annals of Nuclear Energy 18 (9), 535–544.

Muller, E. Z., Wiederhold, A. F., 1995. Selected Non-Linear Iterative Schemes for the Multigroup Analytic Nodal Method. In: Proceedings of the Intl. Conf. on Mathematics and Computation, Reactor Physics, and Environmental Analyses, April 30 - May 4. Portland, Oregan, USA.

Nakamura, S., 1977. Computational Methods in Engineering and Science. John Wiley & Sons, New York.

Noh, J., Cho, N., 1993. A new Diffusion Nodal Method based on Analytical Function Expansion. Trans. Am. Nucl. Soc. 69, 162–163.

Noh, J., Cho, N. Z., 1994. A new approach to the Analytic Function Expansion method to Neutron Diffusion Nodal Calculation. Nucl. Sci. Eng. 116, 165.

O Dell, R. D., Brinkley, F. W., Marr, D., 1982. Users Guide for TWODENT: A Code Package for Two-Dimensional Diffusion - Accelerated Neutral Particle Transport (LA-9814-M). Tech. rep., LANL.

Ougouag, A. M., Rajić, H. L., 1988. ILLICO-HO: a Self-consistent Higher-order coarse-mesh Nodal Method. Nucl. Sci. Eng. 100, 332.

Panayotov, D., 2004. POLCA-T Simulation of OECD/NRC BWR Turbine Trip Benchmark Exercise 3 Best Estimate Scenario TT2 Test and Four Extreme Scenarios. pintassilgo2.ipen.br.

Parsons D. K., Nigg D. W., 1985. Extension of the Analytic Nodal Method to Four Energy Groups (report EGG-PBS-6821). Tech. rep., EG and G Idaho, Inc., Idaho Falls (USA).

Prinsloo, R., Moloko, L., Bokov, P. M., Stander, G., Elsakhawy, K., Theron, S., 2008. SAFARI-1 Benchmark Specification (RRT-SAFARI-08-22). Tech. rep., Necsa.

Prinsloo, R., Tomašević, D. I., 2011. A Practical Implementation of a Higher Order Transverse Leakage Approximation. In: Proceedings of the International Conference on Mathematics and Computation Methods Applied to Nuclear Science and Engineering (May 8-12 2011). Rio de Janeiro, Brazil.

Prinsloo, R. H., 2006. Solution of the Multi-group Analytic Nodal Diffusion Equations in 3-Dimensional Cylindrical Geometry. Msc, North West University (Potchefstroom Campus).

Prinsloo, R. H., Tomašević, D. I., Nov. 2008. The Analytic Nodal Method in Cylindrical Geometry. Nucl. Sci. Eng. 238 (11), 2898–2907.
URL http://linkinghub.elsevier.com/retrieve/pii/S0029549308001271

Prinsloo, R. H., Tomašević, D. I., 2012. Development of Iteration Strategies for a Practical Implementation of a Higher Order Transverse Leakage Approximation. In: Proceedings of PHYSOR 2012: Advances in Reactor Physics Linking Research, Industry and Education (April 15 - 20, 2012). Knoxville, USA.

Rajić, H. L., Ougouag, A. M., 1987. Advanced Nodal Neutron Diffusion method with Space-dependent Cross Sections: ILLICO-VX. Trans. Am. Nucl. Soc. 55 (CONF-8711195-).

Rajić, H. L., Ougouag, A. M., 1989. ILLICO: A Nodal Neutron Diffusion Method for Modern Computer Architectures. Nucl. Sci. Eng. 103 (4).

Rearden, B., Williams, M. L., Jessee, M. A., Mueller, D. E., Wiarda, D. A., 2011. Sensitivity and Uncertainty Analysis Capabilities and Data in SCALE. Nuclear Technology 174, 236–288.

Reitsma, F., Muller, E., 2002. Flexible Exposure and Nodal Mesh Treatment in the 3D Nodal Simulator MGRAC: Application to a MTR Case with Axially Movable Assemblies. Proceedings of PHYSOR 2002, Seoul, Korea, October 7-10.

Reitsma, F., Prinsloo, R. H., Thugwane, S., 2004. Importance of Including Irradiation Rig Loading in Research Reactors Cycle Planning and Core Follow Calculations. In: Proceedings of the 14th Pacific Basin Nuclear Conference, 15-19 March. Honolulu, Hawaii, USA.

Shober, R., 1978. A Nodal Method for Solving Transient Few-group Neutron Diffusion Equations. ANL-78-51.

Shober, R., Henry, A. F., 1976a. Non-linear methods for solving the Diffusion Equation. MIT Report MITNE-196.

Shober, R., Sims, R. N., Henry, A. F., 1977. Two Nodal Methods for Solving Time-dependent Group Diffusion Equations. Nucl. Sci. Eng. 64, 582–592.

Shober, R. A., Henry, A. F., 1976b. An Approximate Analytical Method for Determining Nodal Fluxes. Trans. Am. Nucl. Soc. 24, 192.

Smith, K. S., 1979. An Analytic Nodal Method for Solving the Two-group, Multidimensional, Static and Transient Neutron Diffusion Equations. Ph.D. thesis, M. I. T., Dept. of Nuclear Engineering.

Smith, K. S., 1986. Assembly Homogenization Techniques for Light Water Reactor Analysis. Progress in Nuclear Energy 17 (3), 303–335.

Smith, K. S., 1992. Enhancements of the Studsvik Core Management System (CMS). In: Proceedings of Topical Meeting of Advanced Reactor Physics. Charleston, U.S., pp. 1–117.

Smith, K. S., 1994. Practical and Efficient Iterative method for LWR Fuel Homogenization. Trans. Am. Nucl. Soc. 71, 238.

Smith, K. S., 2003. Reactor Core Methods. Invited lecture at the M&C 2003 International Conference.

Stamm'ler, R. J. J., Abbate, M. J., 1983. Methods of Steady State Reactor Physics in Nuclear Design. Vol. Chapter 5. Academic Press, Great Britain.

Stander, G., Prinsloo, R. H., Müller, E., Tomašević, D. I., 2008. OSCAR-4 Code System Application to the SAFARI-1 Reactor. In: Proceedings of the International Conference on Reactor Physics, Nuclear Power, Interlaken, Switzerland, September 14-19.

Sutton, T. M., 1988. Wielandt Iteration as Applied to the Nodal Expansion Method. Nucl. Sci. Eng. 98, 169–173.

Sutton, T. M., 1989. NODEX: A Higher-order NEM-based Multigroup Nodal Code. In: Proceedings of Advances in nuclear engineering computation and radiation shielding. Sante Fe, NM, USA, p. 16.

Sutton, T. M., Aviles, B. N., 1996. Diffusion Theory methods for Spatial Kinetics Calculations. Progress in Nuclear Energy 30 (2), 119–182.

Tomašević, D. I., 1996. Modern Nodal Diffusion Methods in Nuclear Reactor Analysis and Design. Proceedings of the Yugoslav Nuclear Society Conference, 77.

Tomašević, D. I., 1997. A Consistent Transverse Leakage Approximation. In: Proceedings of the Joint International Conference on Mathematical Methods and Supercomputing for Nuclear Applications. Saratoga, USA, pp. 134 – 139.

Tomašević, D. I., Larsen, E. W., 1993. Benchmarking with High-Order Nodal Diffusion Methods. Trans. Am. Nucl. Soc. 69, 212–214.

Turinsky, P. J., 1994. NESTLE: A Few-Group Neutron Diffusion Equation Solver Utilizing the Nodal Expansion Method for Eigenvalue, Adjoint, Fixed-Source Steady-State and Transient Problems, EGG-NRE-11406. Tech. rep.

Varga, R. S., 1965. Matrix Iterative Analysis (3rd printing). Prentice-Hall, Inc.

Vogel, D. L., 1993. A New Versatile Iteration Algorithm for the Analytic Nodal Method. In: Proceedings of Int. Conf. Mathematical Methods and Supercomputing in Nuclear Applications. Karlsruhe, Germany, April 19 - 23.

Vogel, D. L., Weiss, Z. J., 1992. A General, Multigroup Formulation of the Analytic Nodal Method. Proc. Int. Topical Meeting on Advances in Reactor Physics, Charleston, South Carolina, USA, 8–11.

Wagner, M. R., 1974. Nodal Synthesis Method and Embedded Flux Calculations. Trans. Am. Nucl. Soc. 18, 152.

Wagner, M. R., Koebke, K., Winter, J. H., 1981. A Nonlinear Extension of the Nodal Expansion Method. In: Proc. Conf. Advances in Mathematical Methods for the Solution of Nuclear Engineering Problems. Munich, p. 43.

Woo, S. W., Cho, N. Z., 2000. A Refinement of the Analytic Function Expansin Nodal Method with Transverse Gradient Basis Functions and Interface Flux Moments. In: Proceedings of the International Conference on Advances in Reactor Physics, and Mathematics and Computation Into the Next Millennium. Pittsburgh, USA.

Zhang, H., Rizwan-uddin, Dorning, J. J., 1997. Systematic Homogenization and Self-consistent Flux and Pin Power Reconstruction for Nodal Diffusion Methods. Transport Theory and Statistical Physics 26 (4-5), 433–468.

Appendix A

Weighted transverse integration

A.1 Description of Weighted Transverse Integration in Cartesian Geometry

As the weighted transverse integration approach is adopted in this work in order to develop a practical transverse leakage approximation, the derivation, as in principle described in (Ougouag and Rajić (1988)) is given in quite some detail here. The development produced here does differ somewhat from that which is proposed by Ougouag, since the method was formulated with side-averaged current moments as primary unknowns, where we will build the solution around the traditional ANM structure in which node-averaged fluxes, or in this case, node-averaged flux moments, are the primary unknowns. Further, this appendix serves to introduce notation needed for use in the remainder of this thesis.

As stated before, transverse integration requires that eq. (2.2) is integrated over the two transverse directions, in order to produce a one-dimensional equation in the third direction. This process is repeated for all three directions. To achieve this for a weighted transverse integration approach, it is again convenient to adopt the notation of three arbitrary directions (u, v, w), with u representing the direction of choice and v and w the transverse directions. To produce the set of transversely integrated, one-dimensonal, higher-order nodal equations, eq. (2.2) is multiplied by Legendre polynomials in both transverse directions, of order l and k, respectively. We let l and k range from 0 to M for all combinations of (l, k), where M denotes the order of the method. Note that $M = 0$ denotes the standard lower order equations. Furthermore, I will denote the maximum source expansion order used to formulate the source terms in the one-dimensional equations. Hence, a specific higher-order solution is classified by both indices (M, I). Note that we drop, in this appendix, both the group index g

and the node index n for simplicity. After multiplication then, the resulting equation,

$$-D\left(\bigtriangledown^2\phi(u,v,w)\right)\frac{2k+1}{h_w}P_k(\frac{2w}{h_w})\frac{2l+1}{h_v}P_l(\frac{2v}{h_v})+ \tag{A.1}$$

$$\sigma^{\text{rem}}\phi(u,v,w)\frac{2k+1}{h_w}P_k(\frac{2w}{h_w})\frac{2l+1}{h_v}P_l(\frac{2v}{h_v})$$

$$= Q(u,v,w)\frac{2k+1}{h_w}P_k(\frac{2w}{h_w})\frac{2l+1}{h_v}P_l(\frac{2v}{h_v}) \ ,$$

is integrated over w and then v. Eq. (A.1) is bulky, and we proceed to perform the transverse integration term by term. E.g. the removal term yields, after integration over w,

$$\sigma^{\text{rem}}\frac{2l+1}{h_v}P_l(\frac{2v}{h_v})\frac{2k+1}{h_w}\int_{h_w}\phi(u,v,w)P_k(\frac{2w}{h_w})dw$$

$$= \sigma^{\text{rem}}\frac{2l+1}{h_v}P_l(\frac{2v}{h_v})\phi_k^w(u,v) \tag{A.2}$$

with

$$\phi_k^w(u,v) = \frac{2k+1}{h_w}\int_{h_w}\phi(u,v,w)P_k(\frac{2w}{h_w})dw \ . \tag{A.3}$$

Here we identified $\phi_k^w(u,v)$ as the two-dimensional (u,v) k^{th} semi-moment of the three-dimensional flux. As convention, we shall denote the direction over which a quantity has been integrated via the superscript (w), and the order of the Legendre Polynomial (in that direction) with which it has been folded in the integral, by the corresponding subscript (k). This definition would allow us to express

$$\phi(u,v,w) = \sum_{k=0}^{\infty}\phi_k^w(u,v)P_k(\frac{2w}{h_w}) \approx \sum_{k=0}^{M}\phi_k^w(u,v)P_k(\frac{2w}{h_w}). \tag{A.4}$$

We may complete the transverse integration process by subsequent integration of eq. (A.2) over v to yield:

$$\sigma^{\text{rem}}\frac{2l+1}{h_v}\int_{h_v}\phi_k^w(u,v)P_l(\frac{2v}{h_v})dv = \sigma_{rem}\phi_{lk}^{vw}(u) \tag{A.5}$$

with the double-index (l,k), one-dimensional (u) - flux semi-moment defined as

$$\phi_{lk}^{vw}(u) = \frac{2k+1}{h_v}\int_{h_v}\phi_k^w(u,v)P_l(\frac{2v}{h_v})dv \ . \tag{A.6}$$

Note that the notation has been expanded to indicate that $\phi_{lk}^{vw}(u)$ has been integrated over both w and v. Similarly to eq. (A.4), we may write

$$\phi_k^w(u,v) \approx \sum_{l=0}^{M} \phi_{lk}^{vw}(u) P_l(\frac{2v}{h_v}). \tag{A.7}$$

The process applied to term 2 above may be analogously applied to the source term to yield

$$\frac{2l+1}{h_v}\frac{2k+1}{h_w}\int_{h_v}\int_{h_w} Q(u,v,w)P_k(\frac{2w}{h_w})P_l(\frac{2v}{h_v})dwdv \tag{A.8}$$

$$= \chi^g \frac{1}{k_{\text{eff}}} \sum_{h=1}^{G} \phi_{lk}^{vw,h}(u)\nu\sigma_{\text{fis}}^h + \sum_{h=1,h\neq g}^{G} \phi_{lk}^{vw,h}(u)\sigma_{\text{scat}}^h(h\to g).$$

A.1.1 Higher-order transverse leakage terms

The leakage term in eq. (A.1) is somewhat more involved, and we begin by integrating it in over w to yield

$$-D\left(\bigtriangledown_{uv}^2\phi_k^w(u,v)\right)\frac{2l+1}{h_v}P_l(\frac{2v}{h_v}) - D\frac{2k+1}{h_w}\left(\int_{h_w}\frac{\partial^2\phi(u,v,w)}{\partial w^2}P_k(\frac{2w}{h_w})dw\right)\frac{2l+1}{h_v}P_l(\frac{2v}{h_v}) \tag{A.9}$$

where $\bigtriangledown_{uv}^2 = \frac{\partial^2}{\partial u^2} + \frac{\partial^2}{\partial v^2}$. The integral in the second term needs to be reduced to quantities which are expressible from the solution of the one-dimensional equation (to be formulated later), and we will aim to express all quantities in terms of moments of the side-averaged current, the side-averaged flux or the one-dimensional flux itself. We apply partial integration (twice) to the integral:

$$\int_{h_w}\frac{\partial^2\phi(u,v,w)}{\partial w^2}P_k(\frac{2w}{h_w})dw = \left[P_k(\frac{2w}{h_w})\frac{\partial}{\partial w}\phi(u,v,w)\right]_{-\frac{h_w}{2}}^{\frac{h_w}{2}} - \int_{h_w}\frac{\partial}{\partial w}\phi(u,v,w)P_k'(\frac{2w}{h_w})dw$$

$$= \left[P_k(\frac{2w}{h_w})\frac{\partial}{\partial w}\phi(u,v,w)\right]_{-\frac{h_w}{2}}^{\frac{h_w}{2}} - \left[P_k'(\frac{2w}{h_w})\phi(u,v,w)\right]_{-\frac{h_w}{2}}^{\frac{h_w}{2}} + \int_{h_w}\phi(u,v,w)P_k''(\frac{2w}{h_w})dw. \tag{A.10}$$

The integral in eq. (A.10) contains second order derivatives of Legendre polynomials and we express:

$$P_k''(\frac{2w}{h_w}) = \sum_{t=0}^{k-2} \lambda_{tk}^w P_t(\frac{2w}{h_v}) \tag{A.11}$$

with

$$\lambda_{tk}^w = \frac{2t+1}{h_w} \int_{h_w} P_k''(\frac{2w}{h_w}) P_t(\frac{2w}{h_w}) dw. \tag{A.12}$$

These integrals may be expressed via a recurrence relationship by utilizing partial integration to write (for simplicy in dimensionless coordinate ξ)

$$\lambda_{tk}^{\xi} = \int_{-1}^{1} P_k''(\xi) P_t(\xi) d\xi = P_k'(\xi) P_t(\xi)|_{-1}^{1} - \int_{-1}^{1} P_k'(\xi) P_t'(\xi) d\xi \tag{A.13}$$

$$= \left(\frac{k(k+1)}{2} \right) \left(1 - (-1)^{k+t+1} \right) - \int_{-1}^{1} P_k'(\xi) P_t'(\xi) d\xi$$

for $t \leq k+2$. Similarly we express, by considering:

$$\int_{-1}^{1} P_t''(\xi) P_k(\xi) d\xi = \left(\frac{t(t+1)}{2} \right) \left(1 - (-1)^{k+t+1} \right) - \int_{-1}^{1} P_t'(\xi) P_k'(\xi) d\xi. \tag{A.14}$$

We notice that, due to the orthogonality of Legendre polynomials (and the fact that $k \geq t-2$), that $\int_{-1}^{1} P_t''(\xi) P_k(\xi) d\xi = 0$ and as such we may use eq. (A.14) to eliminate the term $\int_{-1}^{1} P_k'(\xi) P_t'(\xi) d\xi$ from eq. (A.13). This yields, after reverting back to the original coordinate system:

$$\lambda_{tk}^w = \left(\frac{2}{h_w} \right)^2 \left(\frac{2t+1}{2} \right) \left(\frac{k(k+1) - t(t+1)}{2} \right) \left(1 + (-1)^{k+t} \right) \tag{A.15}$$

and thus we may consider the λ_{tk}^w moments known up to an arbitrary order $(k-2)$.

If we now replace eqs. (A.11) and (A.12) into eq. (A.10) into and eq. (A.10) into eq. (A.9), we obtain

$$\frac{2l+1}{h_v} P_l(\frac{2v}{h_v}) \Bigg\{ -D \bigtriangledown_{uv}^2 \phi_k^w(u,v) + \left[\frac{2k+1}{h_w} \left(J^w(u,v,\frac{h_w}{2}) + (-1)^k J^w(u,v,-\frac{h_w}{2}) \right) \right] + \tag{A.16}$$

$$D \frac{2k+1}{h_w} \left[P_k'(\frac{2w}{h_w}) \phi(u,v,w) \right]_{-\frac{h_w}{2}}^{\frac{h_w}{2}} - D \sum_{t=0}^{k-2} \frac{2k+1}{2t+1} \lambda_{tk}^w \phi_t^w(u,v) \Bigg\}$$

with currents defined as

$$J^w(u,v,\frac{h_w}{2}) = -D \frac{\partial}{\partial w} \phi(u,v,\frac{h_w}{2})$$

and

$$J^w(u,v,-\frac{h_w}{2}) = +D\frac{\partial}{\partial w}\phi(u,v,-\frac{h_w}{2}).$$

Here we have used the Legendre polynomial properties:

$$P_k(1) = 1 \ , \ P_k(1) = (-1)^k.$$

Similarly, for the derivative of Legendre polynomials, we apply

$$P_k'(\frac{2w}{h_w})\Big|_{\frac{h_w}{2}} = \frac{2}{h_w}\frac{k(k+1)}{2}$$

and

$$P_k'(\frac{2w}{h_w})\Big|_{-\frac{h_w}{2}} = \frac{2}{h_w}\frac{k(k+1)}{2}(-1)^{k+1}$$

to yield

$$\frac{2l+1}{h_v}P_l(\frac{2v}{h_v})\Bigg\{-D\bigtriangledown_{uv}^2\phi_k^w(u,v) + \left[\frac{2k+1}{h_w}\left(J^w(u,v,\frac{h_w}{2}) + (-1)^k J^w(u,v,-\frac{h_w}{2})\right)\right] + \tag{A.17}$$

$$\frac{D(2k+1)k(k+1)}{h_w^2}\left(\phi(u,v,\frac{h_w}{2}) + (-1)^k\phi(u,v,-\frac{h_w}{2})\right)$$

$$-D\sum_{t=0}^{k-2}\frac{2k+1}{2t+1}\lambda_{tk}^w\phi_t^w(u,v)\Bigg\}.$$

Eq. (A.17) represents the weighted leakage term integrated over w. In order to proceed with the v integration, and manage the large resulting equation, we rewrite the transversely integrated leakage term obtained thus far. We will introduce the more traditional transverse leakage notation, but extend it somewhat to handle the multi-dimensionality of the quantities. Three, comma separated, superscripts may be used. The first denotes the directions over which a given quantity has been integrated, the second the direction for which a given quantity is applicable, and the third (if present) denotes a term descriptor used largely for breaking large expression into smaller separate components. The subscripts still denote the indices of the chosen orders of the Legendre polynomials over which quantities have been folded. Hence, the transversely integrated leakage term may be expressed as:

$$\frac{2l+1}{h_v}\frac{2k+1}{h_w}\int_{h_v}P_l(\frac{2v}{h_v})\int_{h_w}-D\bigtriangledown^2\phi(u,v,w)P_k(\frac{2w}{h_w})dwdv \tag{A.18}$$

$$= \frac{2l+1}{h_v} \int_{h_v} P_l(\frac{2v}{h_v}) \left(-D \bigtriangledown_{uv}^2 \phi_k^w(u,v) + L_k^{w,w}(u,v)\right) dv$$

where we define

$$\bigtriangledown^2 \phi(u,v,w) = \left(\bigtriangledown_u^2 + \bigtriangledown_v^2 + \bigtriangledown_w^2\right) \phi(u,v,w),$$
$$\bigtriangledown_{uv}^2 = \bigtriangledown_u^2 + \bigtriangledown_v^2$$

with

$$L_k^{w,w}(u,v) = L_k^{w,w,\text{cur}}(u,v) + L_k^{w,w,\text{flux}}(u,v) - L_k^{w,w,\text{mom}}(u,v),$$
$$L_k^{w,w,\text{cur}}(u,v) = \frac{2k+1}{h_w} \left(J^w(u,v,\frac{h_w}{2}) + (-1)^k J^w(u,v,-\frac{h_w}{2}) \right),$$

$$L_k^{w,w,\text{flux}}(u,v) = \frac{D(2k+1)k(k+1)}{h_w^2} \left(\phi(u,v,\frac{h_w}{2}) + (-1)^k \phi(u,v,-\frac{h_w}{2}) \right)$$

and

$$L_k^{w,w,\text{mom}}(u,v) = D \sum_{t=0}^{k-2} \frac{2k+1}{2t+1} \lambda_{tk}^w \phi_t^w(u,v).$$

Here we have broken the transverse leakage contribution from w to (u,v) into three components, based on contributions from side currents, side fluxes and explicit flux moments, respectively. If we now perform the v integration in eq. (A.18), we find:

$$\frac{2l+1}{h_v} \frac{2k+1}{h_w} \int_{h_v} \int_{h_w} -D \bigtriangledown^2 \phi(u,v,w) P_k(\frac{2w}{h_w}) P_l(\frac{2v}{h_v}) dw dv \qquad \text{(A.19)}$$
$$= \left(-D \bigtriangledown_u^2 \phi_{lk}^{vw}(u) + L_{lk}^{vw,w}(u) + L_{lk}^{vw,v}(u)\right)$$

with

$$L_{lk}^{vw,w}(u) = L_{lk}^{vw,w,\text{cur}}(u) + L_{lk}^{vw,w,\text{flux}}(u) - L_{lk}^{vw,w,\text{mom}}(u),$$

$$L_{lk}^{vw,v}(u) = L_{lk}^{vw,v,\text{cur}}(u) + L_{lk}^{vw,v,\text{flux}}(u) - L_{lk}^{vw,v,\text{mom}}(u),$$

and

$$L_{lk}^{vw,w,\text{cur}}(u) = \frac{2k+1}{h_w} \left(J_l^{v,w}(u,\frac{h_w}{2}) + (-1)^k J_l^{v,w}(u,-\frac{h_w}{2}) \right)$$

$$L_{lk}^{vw,w,\text{flux}}(u) = \frac{D(2k+1)k(k+1)}{h_w^2} \left(\phi_l^{v,w}(u,\frac{h_w}{2}) + (-1)^l \phi_l^{v,w}(u,-\frac{h_w}{2}) \right)$$

$$L_{lk}^{vw,w,\mathrm{mom}}(u) = \frac{2l+1}{h_v}\int_{h_v} D\sum_{t=0}^{k-2}\frac{2k+1}{2t+1}\lambda_{tk}^{w}\phi_t^{w}(u,v)P_l(\frac{2v}{h_v})dv$$

$$= D\sum_{t=0}^{k-2}\frac{2k+1}{2t+1}\lambda_{tk}^{w}\phi_{tl}^{wv}(u).$$

Here, as an example of the newly introduced notation, $L_{kl}^{wv,w,\mathrm{cur}}(u)$ denotes the (w,v)-integrated transverse leakage contribution from w to u, and then specifically the current(cur) contribution to the full leakage term.

We now proceed to the contribution of the $v-$component of the Laplacian term. The contribution from v to the transverse leakage ($L_{kl}^{wv,v}(u)$) retains the form of the w contribution ($L_{kl}^{wv,w}(u)$) which is explicitly given above, and takes the form

$$L_{kl}^{wv,v,\mathrm{cur}}(u) = \left[\frac{2l+1}{h_v}\left(J_k^{w,v}(u,\frac{h_v}{2}) + (-1)^l J_k^{w,v}(u,-\frac{h_v}{2})\right)\right] \tag{A.20}$$

with

$$J_k^{w,v}(u,\pm\frac{h_v}{2}) = \mp D\frac{\partial}{\partial v}\phi_k^{w}(u,\pm\frac{h_v}{2}),$$

$$L_{kl}^{wv,v,\mathrm{flux}}(u) = \frac{D(2l+1)l(l+1)}{h_v^2}\left(\phi_k^{w,v}(u,\frac{h_v}{2}) + (-1)^l\phi_k^{w,v}(u,-\frac{h_v}{2})\right) \tag{A.21}$$

and

$$L_{kl}^{wv,v,\mathrm{mom}}(u) = D\sum_{t=0}^{l-2}\frac{2l+1}{2t+1}\lambda_{tl}^{v}\phi_{tk}^{vw}(u) \tag{A.22}$$

This expression completes the transverse integration process, and yields a u- dependent, one-dimensional ordinary, inhomogeneous differential equation, with double-index flux moments in u-direction as unknowns. If we assemble all relevant terms, the final equation therefore is

$$-D\frac{d}{du^2}\phi_{lk}^{vw}(u) + \sigma^{\mathrm{rem}}\phi_{lk}^{vw}(u) = \chi^g\frac{\nu}{k_{\mathrm{eff}}}\sum_{h=1}^{G}\phi_{lk}^{vw,h}(u)\sigma_{\mathrm{fis}}^{h} + \tag{A.23}$$

$$\sum_{h=1,h\neq g}^{G}\phi_{lk}^{vw,h}(u)\sigma_{\mathrm{scat}}^{h}(h\to g) - L_{lk}^{vw,w}(u) - L_{lk}^{vw,v}(u)$$

with

$$L_{lk}^{vw,w}(u) = \frac{2k+1}{h_w}\left(J_l^{v,w}(u,\frac{h_w}{2}) + (-1)^k J_l^{v,w}(u,-\frac{h_w}{2})\right) +$$

$$\frac{D(2k+1)k(k+1)}{h_w^2}\left(\phi_l^{v,w}(u,\frac{h_w}{2}) + (-1)^k\phi_l^{v,w}(u,-\frac{h_w}{2})\right) - D\sum_{t=0}^{k-2}\frac{2k+1}{2t+1}\lambda_{tk}^{w}\phi_{lt}^{vw}(u)$$

and

$$L_{lk}^{vw,v}(u) = \frac{2l+1}{h_v}\left(J_k^{w,v}(u,\frac{h_v}{2}) + (-1)^l J_k^{w,v}(u,-\frac{h_v}{2})\right) +$$

$$\frac{D(2l+1)l(l+1)}{h_v^2}\left(\phi_k^{w,v}(u,\frac{h_v}{2}) + (-1)^l\phi_k^{w,v}(u,-\frac{h_v}{2})\right) - D\sum_{t=0}^{l-2}\frac{2l+1}{2t+1}\lambda_{lt}^v\phi_{tk}^{vw}(u).$$

A.1.2 Solution of the one-dimensional higher-order equations

At this point we make the observation that eq. (A.23) has assumed the same form as eq. (2.5), and as such will assume the same form of solution described in Section 2.3.2.1. Nevertheless, for the sake of completion, we repeated some of the steps here. Equation (A.23) becomes, in dimension coordinates ξ:

$$\frac{d}{d\xi^2}\phi_{lk}^{vw}(\xi) + (\beta^{nm})^2\,\phi_{kl}^{wv}(\xi) = Q_{lk}^{vw}(\xi), \tag{A.24}$$

$$(\beta^{mn})^2 = \left(\frac{h_u}{2}\right)^2\frac{\sigma^{\text{rem}}}{-D}$$

with

$$Q_{lk}^{vw}(\xi) = -\frac{1}{D}\left(\frac{h_u}{2}\right)^2\left(\chi\frac{\nu^g}{k_{\text{eff}}}\sum_{h=1}^{G}\phi_{lk}^{vw,h}(\xi)\sigma_{\text{fis}}^h + \sum_{h=1,h\neq g}^{G}\phi_{lk}^{vw,h}(\xi)\sigma_{\text{scat}}^h(h\to g)\right.$$

$$\left. - L_{lk}^{vw,w}(\xi) - L_{lk}^{vw,v}(\xi)\right)$$

$$L_{lk}^{vw,w}(\xi) = \frac{2(2k+1)}{h_w^2}\left(J_l^{v,w}(\xi,1) + (-1)^k J_l^{v,w}(\xi,-1)\right) +$$

$$\frac{D(2k+1)k(k+1)}{h_w^2}\left(\phi_l^v(\xi,1) + (-1)^k\phi_l^v(\xi,-1)\right) - D\sum_{t=0}^{k-2}\frac{2k+1}{2t+1}\lambda_{tk}^w\phi_{lt}^{vw}(\xi)$$

and

$$L_{lk}^{vw,v}(\xi) = \frac{2(2l+1)}{h_v^2}\left(J_k^{w,v}(\xi,1) + (-1)^l J_k^{w,v}(\xi,-1)\right) +$$

$$\frac{D(2l+1)l(l+1)}{h_v^2}\left(\phi_k^w(\xi,1) + (-1)^l\phi_k^w(\xi,-1)\right) - D\sum_{t=0}^{l-2}\frac{2l+1}{2t+1}\lambda_{tl}^v\phi_{tk}^{vw}(\xi).$$

In order to solve eq. (A.24), it is useful to express the right hand side in terms of a Legendre expansion. This requires that each of the fission, scattering and leakage sources are individually expressed in terms of a u-dependent Legendre expansion.

The detail hereof will be handled in A.1.3, and we assume for the moment that $Q_{lk}^{vw}(\xi) = \sum_{i=0}^{I} d_{ilk}^{uvw} P_i(\xi)$ is known. Here we have limited the source expansion to order I. The analytic solution of eq. (A.24) may be expressed as

$$\phi_{lk}^{vw}(\xi) = A_{lk}\cosh(|\beta^{nm}|\,\xi) + B_{lk}\sinh(|\beta^{nm}|\,\xi) + \sum_{i=0}^{I} b_{ilk}^{uvw} P_i(\xi). \tag{A.25}$$

We have expressed the moments of the particular solution (b_i) in terms of the moments of the source (d_i) via the following recurrence relation:

$$\begin{aligned} b_I &= \tfrac{1}{(|\beta^{nm}|)^2}(\tfrac{h_u}{2})^2 D^{-1} d_I \\ b_{I-1} &= \tfrac{1}{(|\beta^{nm}|)^2}(\tfrac{h_u}{2})^2 D^{-1} d_{I-1} \\ b_i &= \tfrac{1}{(|\beta^{nm}|)^2}\left[(\tfrac{h_u}{2})^2 D^{-1} d_i - \sum_{m=i+2}^{I} a_{im} b_m\right], \qquad i = I-2, \ldots 1, 0 \end{aligned} \tag{A.26}$$

with

$$a_{im} = \frac{2i+1}{4}\left[1 + (-1)^{i+m}\right]\left[m(m+1) - i(i+1)\right],$$

which is obtained by utilizing the orthogonality of Legendre polynomials. Note that in eq. (A.26) we have dropped the superscripts (uvw) and subscripts (ilk) for clarity.

A.1.3 Source moments of the one-dimensional equation

The higher-order source moments (d_{ilk}^{wvu}), which consist of contributions from the higher-order fission source moments, higher-order scattering source moments and higher-order leakage moments are typically expressed in terms of higher-order moments of the flux, current and side-flux from the previous iteration.

A.1.3.1 Higher-order flux moments

Legendre moments have to be developed for one-dimensional double index higher-order fluxes. These higher-order flux moments are similar in form to zero-order moments in the standard nodal methods, and thus may be calculated as

$$\phi_{lk}^{vw}(\xi) = \sum_{i=0}^{I} \phi_{ilk}^{uvw} P_i(\xi), \tag{A.27}$$

with

$$\phi_{ilk}^{uvw} = \frac{2i+1}{2}\int_{-1}^{1}\phi_{lk}^{vw}(\xi)P_i(\xi)d\xi \tag{A.28}$$

$$= \frac{2i+1}{2}\left(A_{lk}\int_{-1}^{1}\cosh(|\beta^{nm}|\,\xi)P_i(\xi)d\xi + B_{lk}\int_{-1}^{1}\sinh(|\beta^{nm}|\,\xi)P_i(\xi)d\xi + b_{ilk}^{uvw}\right). \tag{A.29}$$

Each of the integrals in eq. (A.29) are solvable via recurrence relations and we write

$$\phi_{ilk}^{uvw} = \frac{2i+1}{2}\left(A_{lk}f_i^{\cos} + B_{lk}f_i^{\sin} + b_{ilk}^{uvw}\right)$$

with the expressions for $f_i^{\cos}$ and $f_i^{\sin}$ derived in Appendix C. These flux moments are the needed constituents for expressing the higher-order (and lower-order for that matter) fission source and higher-order scattering source moments in eq. (A.24). It now remains to express the transverse leakage source Legendre expansion in terms of available quantities.

A.1.3.2 Higher-order transverse leakage source moments

We express the higher-order transverse leakage source in terms of a Legendre expansion as

$$L_{lk}^{vw,w}(\xi) = \sum_{i=0}^{I} L_{ilk}^{uvw,w}P_i(\xi)$$

and

$$L_{lk}^{vw,v}(\xi) = \sum_{i=0}^{I} L_{ilk}^{uvw,v}P_i(\xi).$$

Fully expanded, this yields

$$L_{ilk}^{uvw,w} = \frac{2(2k+1)}{h_w^2}\left(J_{il}^{uv,w}(+1) + (-1)^k J_{il}^{uv,w}(-1)\right) + \tag{A.30}$$

$$\frac{D(2k+1)k(k+1)}{h_w^2}\left(\phi_{il}^{uv,w}(+1) + (-1)^k\phi_{il}^{uv,w}(-1)\right) - D\sum_{t=0}^{k-2}\frac{2k+1}{2t+1}\lambda_{tk}^{w}\phi_{ilt}^{uvw}$$

and

$$L_{kli}^{wvu,v} = \frac{2(2l+1)}{h_v^2}\left(J_{ki}^{wu,v}(+1) + (-1)^l J_{ki}^{wu,v}(-1)\right) + \tag{A.31}$$

$$\frac{D(2l+1)l(l+1)}{h_v^2}\left(\phi_{ki}^{wu,v}(+1) + (-1)^l \phi_{ki}^{wu,v}(-1)\right) - D\sum_{t=0}^{l-2}\frac{2l+1}{2t+1}\lambda_{lt}^{v}\phi_{itk}^{uvw}.$$

We may notice that we need higher-order moments of the current from the transverse directions ($J_{il}^{uv,w}(\pm 1)$ and $J_{ki}^{wu,v}(\pm 1)$), higher-order moments of side-flux from the transverse directions ($\phi_{il}^{uv,w}(\pm 1)$ and $\phi_{ki}^{wu,v}(\pm 1)$) and finally higher moments of the flux (ϕ_{ilt}^{uvw} and ϕ_{itk}^{uvw}). Higher-order flux moments were constructed in Section A.1.3.1, and thus it remains to resolve the needed expressions for the higher-order net current and higher-order side-fluxes. To achieve this, we construct a two node problem in order to determine the higher-order interface fluxes and higher-order interface currents, in an analogous way to the procedure followed in the case of the zero order quantities, as described in Section 2.3.2.2.

A.1.4 Higher-order balance equation

In solving the two node problem on each surface, with the aim of determining the higher-order side-current and higher-order side-flux moments, the node-averaged value of the higher-order flux moments are required (see eq. (2.19) when applied to the higher-order equations). The node-averaged higher-order flux moments are typically determined via the solution of the set of coupled higher-order balance equations. The set of higher-order balance equations, with triple index flux moments as primary unknowns, are generated by multiplying eq. (A.23) with $P_i(u)$ and integrating it over u. The resulting set of equations contain higher-order node averaged flux moments, side-flux moments and side-current moments and techniques analogous to those described in Section 2.3.2.2 are used to eliminate two of these in favour of the other. As we do not require the formulation of the higher-order balance equations, as discussed in Chapter 3 in this development, their explicit form is not assembled here.

Appendix B

Additional benchmark problem results

This appendix contains detailed results and information regarding each of the benchmark problems discussed in this work. In particular, relative power density reference results are provided for each problem, as well as error distributions for selected cases. Where applicable flux results are also provided.

B.1 3D MOX C5 Benchmark Problem

For the 3D MOX C5 problem, the assembly averaged distributions provide a good indicator for the error distributions. The reference and error related results are thus presented in Table B.1, for brevity, for assembly averaged quantities only. The table contains results for relative power density, fast flux and thermal flux distributions and shows SQLA and CQLA errors in terms of associated databars. Flux results are normalized to a total reactor power of 1.

Table B.1: Reference results for the 3D MOX C5 benchmark, with SQLA and CQLA percentage errors indicated in databar format in each cell.

Assembly Averaged Fast Flux

	1	2	3
C	1.225E-04 0.13 0.19	8.013E-05 0.04 0.07	7.418E-06 0.87 0.24
B	8.013E-05 0.04 0.07	4.207E-05 0.44 0.04	3.613E-06 0.50 0.35
A	7.418E-06 0.87 0.24	3.613E-06 0.50 0.35	4.094E-07 12.55 2.51

Reference
SQLA % error
CQLA % error

Relative assembly power dens.

	1	2	3
C	1.3380 0.03 0.16	1.0950 0.15 0.08	
B	1.0950 0.15 0.08	0.4712 0.60 0.06	
A			

Assembly Averaged Thermal Flux

	1	2	3
C	2.537E-05 0.00 0.15	6.666E-06 0.08 0.13	7.104E-06 0.86 0.33
B	6.666E-06 0.08 0.13	8.979E-06 0.63 0.08	3.827E-06 0.05 0.59
A	7.104E-06 0.86 0.33	3.827E-06 0.05 0.59	5.699E-07 13.21 0.86

B.2 2D IAEA LWR Benchmark Problem

The reference relative power density distribution for this problem, as calculated with HOTR in FHO_6 mode is given in Table B.2. Included in the table, as databars below each reference value, are the SQLA and CQLA percentage relative power density errors.

Table B.2: Reference relative power density results for the 2D IAEA LWR benchmark, with SQLA and CQLA percentage errors indicated with in databar format in each cell.

	1	2	3	4	5	6	7	8
H	0.7549 0.15 0.03	0.7357 0.40 0.07	0.6922 0.54 0.04					Reference SQLA % error CQLA % error
G	0.9343 0.00 0.00	0.9503 0.02 0.00	0.9750 0.08 0.09	0.8462 0.46 0.06	0.5972 0.91 0.02			
F	0.9351 0.01 0.02	1.0360 0.11 0.00	1.0700 0.01 0.04	0.9064 0.19 0.03	0.6855 0.77 0.16	0.5850 0.20 0.09		
E	0.6100 0.07 0.05	1.0700 0.09 0.05	1.1790 0.07 0.01	0.9670 0.06 0.02	0.4706 0.22 0.01	0.6855 0.77 0.16	0.5972 0.91 0.02	
D	1.2110 0.36 0.04	1.3150 0.25 0.04	1.3450 0.06 0.03	1.1930 0.08 0.03	0.9670 0.06 0.02	0.9064 0.19 0.03	0.8462 0.46 0.06	
C	1.4540 0.54 0.05	1.4800 0.27 0.06	1.4690 0.18 0.01	1.3450 0.06 0.03	1.1790 0.07 0.01	1.0700 0.01 0.04	0.9750 0.08 0.09	0.6922 0.54 0.04
B	1.3100 0.48 0.07	1.4350 0.39 0.04	1.4800 0.27 0.06	1.3150 0.25 0.04	1.0700 0.09 0.05	1.0360 0.11 0.00	0.9503 0.02 0.00	0.7357 0.40 0.07
A	0.7456 0.06 0.08	1.3100 0.48 0.07	1.4540 0.54 0.05	1.2110 0.36 0.04	0.6100 0.07 0.05	0.9351 0.01 0.02	0.9343 0.00 0.00	0.7549 0.15 0.03

The fast and thermal reference flux distribution and associated SQLA and CQLA percentage flux errors are given in Tables B.3 and B.4. The total power of the reactor is set to the total fuel volume.

Table B.3: Reference fast flux results for the 2D IAEA LWR benchmark, with SQLA and CQLA percentage errors indicated with in databar format in each cell.

	1	2	3	4	5	6	7	8	9
	3.370E+00	3.220E+00	2.438E+00	7.106E-01					Reference
	0.32	0.29	0.06	5.70					SQLA % error
I	0.06	0.16	0.42	0.49					CQLA % error
	2.033E+01	1.985E+01	1.666E+01	5.952E+00	2.421E+00	5.717E-01			
	0.10	0.29	0.28	0.21	1.67	8.12			
H	0.01	0.04	0.05	0.23	0.42	0.73			
	2.941E+01	2.984E+01	2.909E+01	2.259E+01	1.444E+01	3.994E+00	6.411E-01		
	0.03	0.07	0.07	0.35	0.56	0.19	9.89		
G	0.00	0.00	0.00	0.04	0.12	0.40	0.24		
	2.994E+01	3.273E+01	3.370E+01	2.850E+01	2.076E+01	1.402E+01	3.994E+00	5.717E-01	
	0.02	0.12	0.02	0.17	0.71	0.05	0.19	8.12	
F	0.02	0.03	0.02	0.01	0.10	0.12	0.40	0.73	
	2.656E+01	3.422E+01	3.721E+01	3.090E+01	2.039E+01	2.076E+01	1.444E+01	2.421E+00	
	0.16	0.07	0.04	0.05	0.16	0.71	0.56	1.67	
E	0.03	0.03	0.00	0.00	0.00	0.10	0.12	0.42	
	3.870E+01	4.154E+01	4.245E+01	3.768E+01	3.090E+01	2.850E+01	2.259E+01	5.952E+00	7.106E-01
	0.33	0.25	0.08	0.07	0.05	0.17	0.35	0.21	5.70
D	0.04	0.05	0.04	0.02	0.00	0.01	0.04	0.23	0.49
	4.588E+01	4.670E+01	4.637E+01	4.245E+01	3.721E+01	3.370E+01	2.909E+01	1.666E+01	2.438E+00
	0.48	0.28	0.21	0.08	0.04	0.02	0.07	0.28	0.06
C	0.04	0.04	0.04	0.04	0.00	0.02	0.00	0.05	0.42
	4.189E+01	4.533E+01	4.670E+01	4.154E+01	3.422E+01	3.273E+01	2.984E+01	1.985E+01	3.220E+00
	0.42	0.39	0.28	0.25	0.07	0.12	0.07	0.29	0.29
B	0.04	0.04	0.04	0.05	0.03	0.03	0.00	0.04	0.16
	3.247E+01	4.189E+01	4.588E+01	3.870E+01	2.656E+01	2.994E+01	2.941E+01	2.033E+01	3.370E+00
	0.10	0.42	0.48	0.33	0.16	0.02	0.03	0.10	0.32
A	0.08	0.04	0.04	0.04	0.03	0.02	0.00	0.01	0.06

Table B.4: Reference thermal flux results for the 2D IAEA LWR benchmark, with SQLA and CQLA percentage errors indicated with in databar format in each cell.

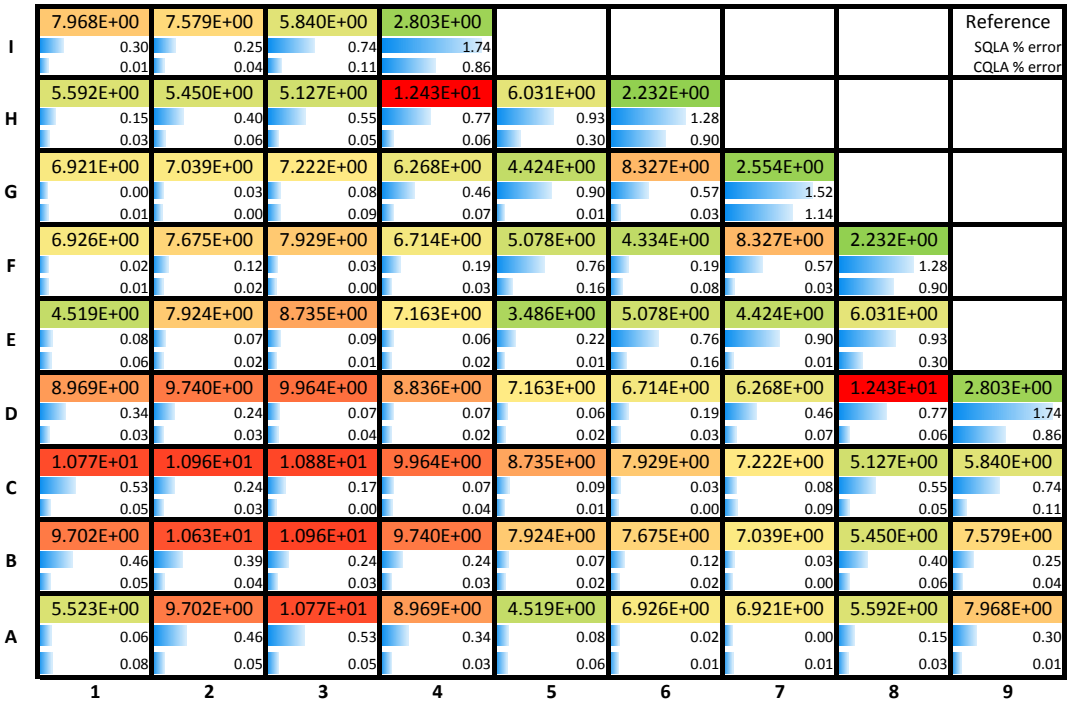

B.3 3D IAEA LWR Benchmark Problem

This section provides additional results and comparisons for the 3D version of the IAEA LWR benchmark problem. As discussed in Section 5.3.2, some doubt exists regarding the convergence of the original published reference results as found in (Lee, 1977). In order to clarify this, we present in Tables B.5 - B.21, a complete nodal power density comparison between the originally published reference result and the HOTR FHO_6 result (which we employ as reference in this work). In order to confirm that the HOTR-FHO_6 is indeed the true reference, the following was taken into account:

- Published results from full higher order codes support the HOTR k_{eff} of 1.02907 (as compared to 1.02903 from (Lee, 1977));
- An independent full higher order calculation, using a 3D version of the CASTOR code as described in Tomašević and Larsen (1993), confirmed that the HOTR result correctly produced the full sixth order calculational result; and

- An independent fine mesh calculation with the OSCAR-4 (Stander et al., 2008) code, utilizing SQLA with an 8 times refined nodal mesh, confirmed the HOTR result to within 0.2%, which is much smaller than the obtained differences as compared to the published reference.

Tables B.5 - B.21 then provide layer by layer (18 to 2 numbered bottom to top) reference results for the nodal power density distribution between the originally published reference, the HOTR FHO_6 result and the HOTR CQLA result. In these tables only the one-eight symmetry segment is shown. It can be seen that the original fine-mesh finite-difference reference solution has nodal power errors of close to 2% distributed throughout the top and bottom layers of the problem.

Table B.5: Comparison for IAEA 3D LWR benchmark between published reference, HOTR reference and CQLA power density results for axial layer 18.

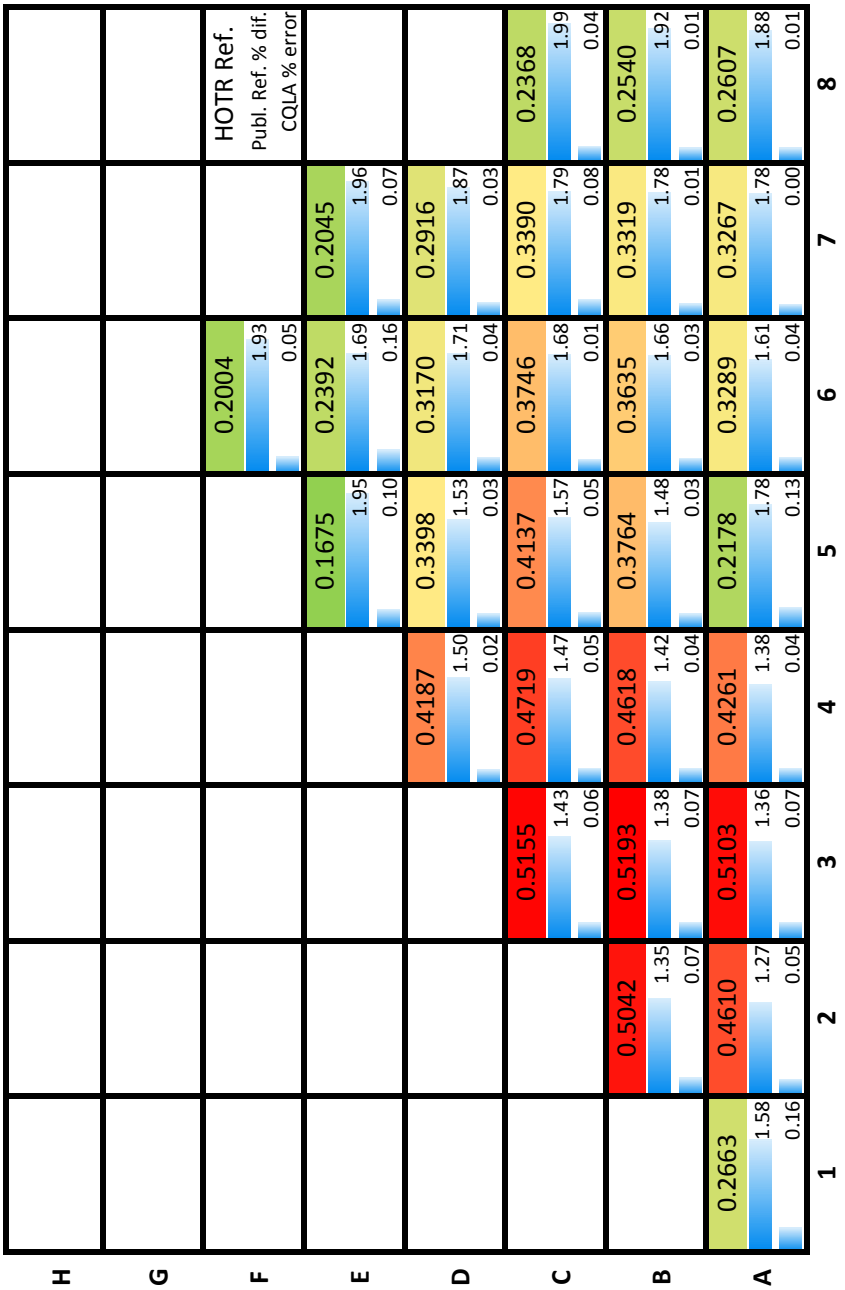

Table B.6: Comparison for IAEA 3D LWR benchmark between published reference, HOTR reference and CQLA power density results for axial layer 17.

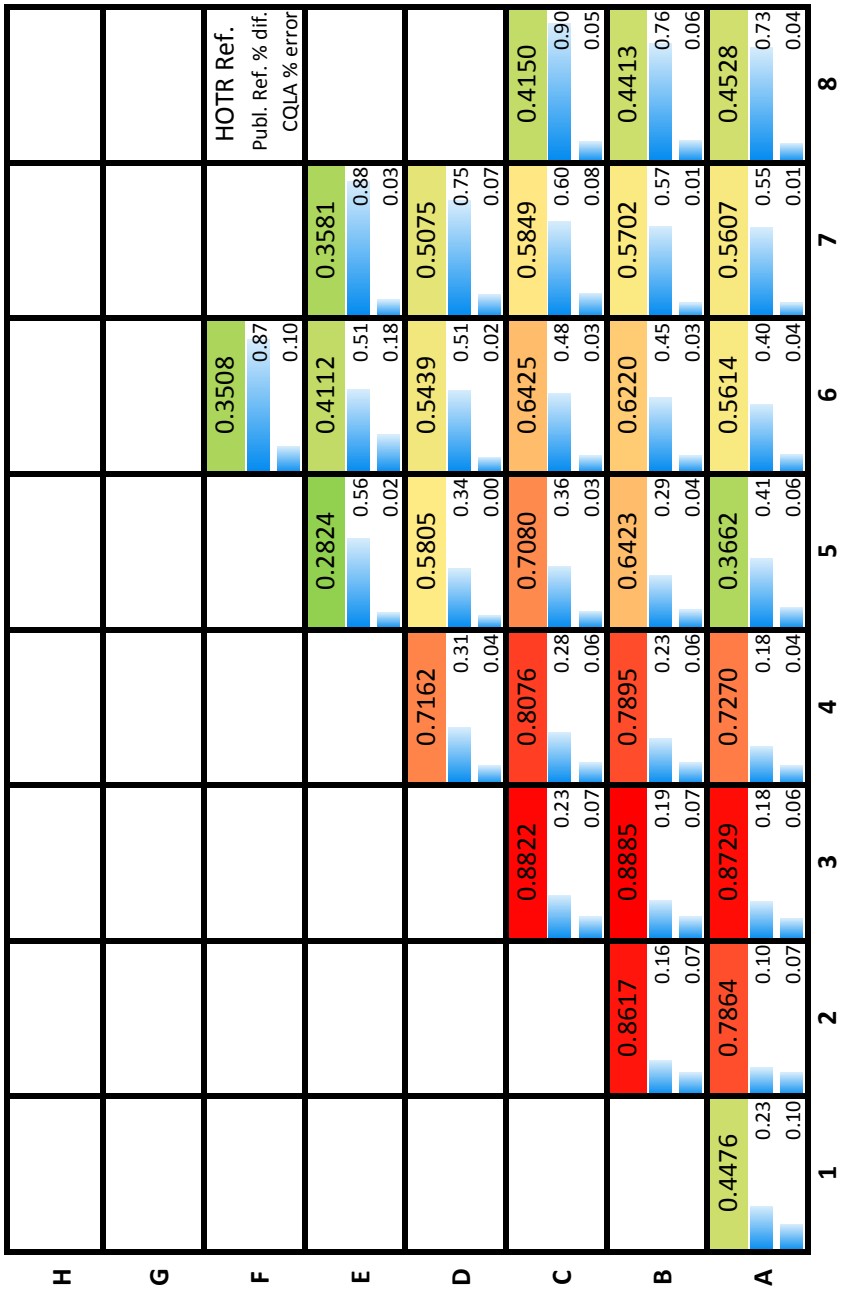

Table B.7: Comparison for IAEA 3D LWR benchmark between published reference, HOTR reference and CQLA power density results for axial layer 16.

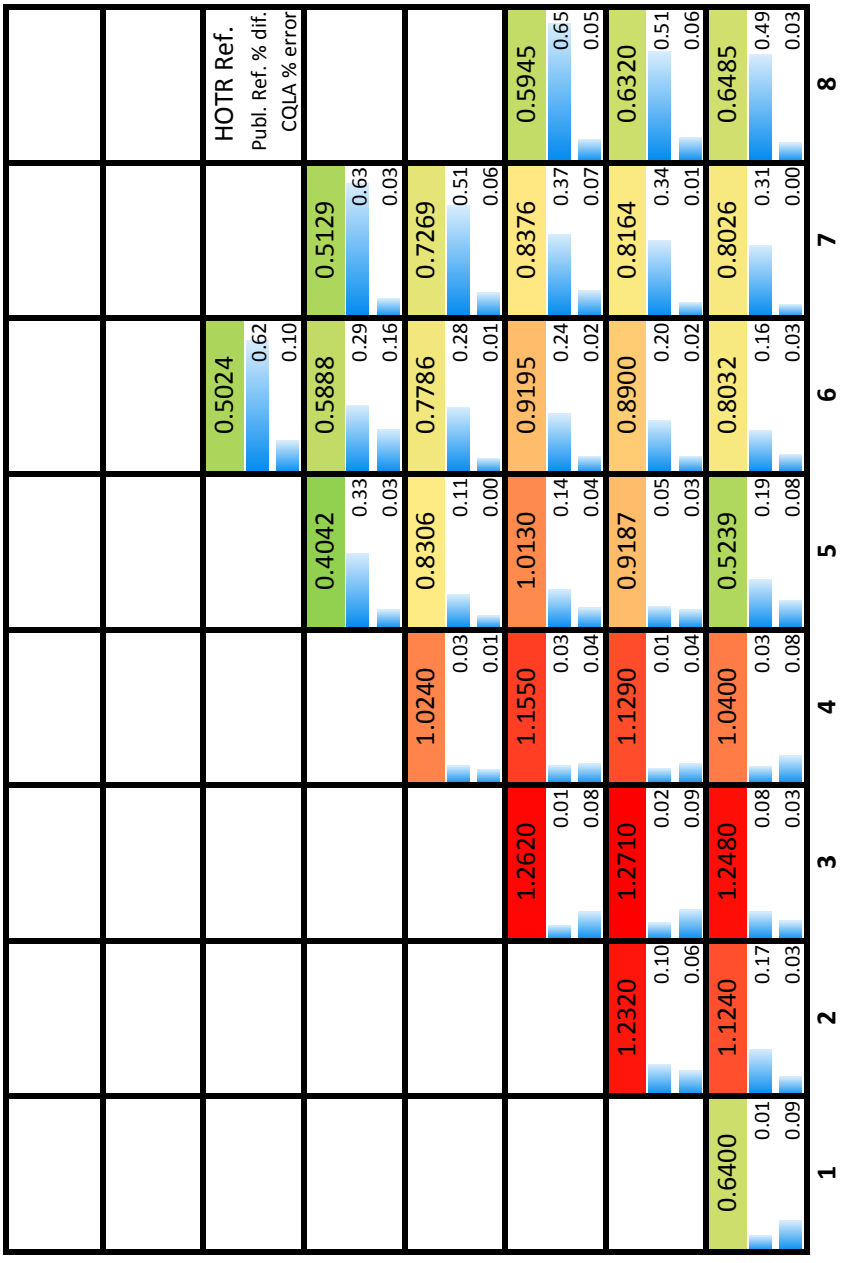

Table B.8: Comparison for IAEA 3D LWR benchmark between published reference, HOTR reference and CQLA power density results for axial layer 15.

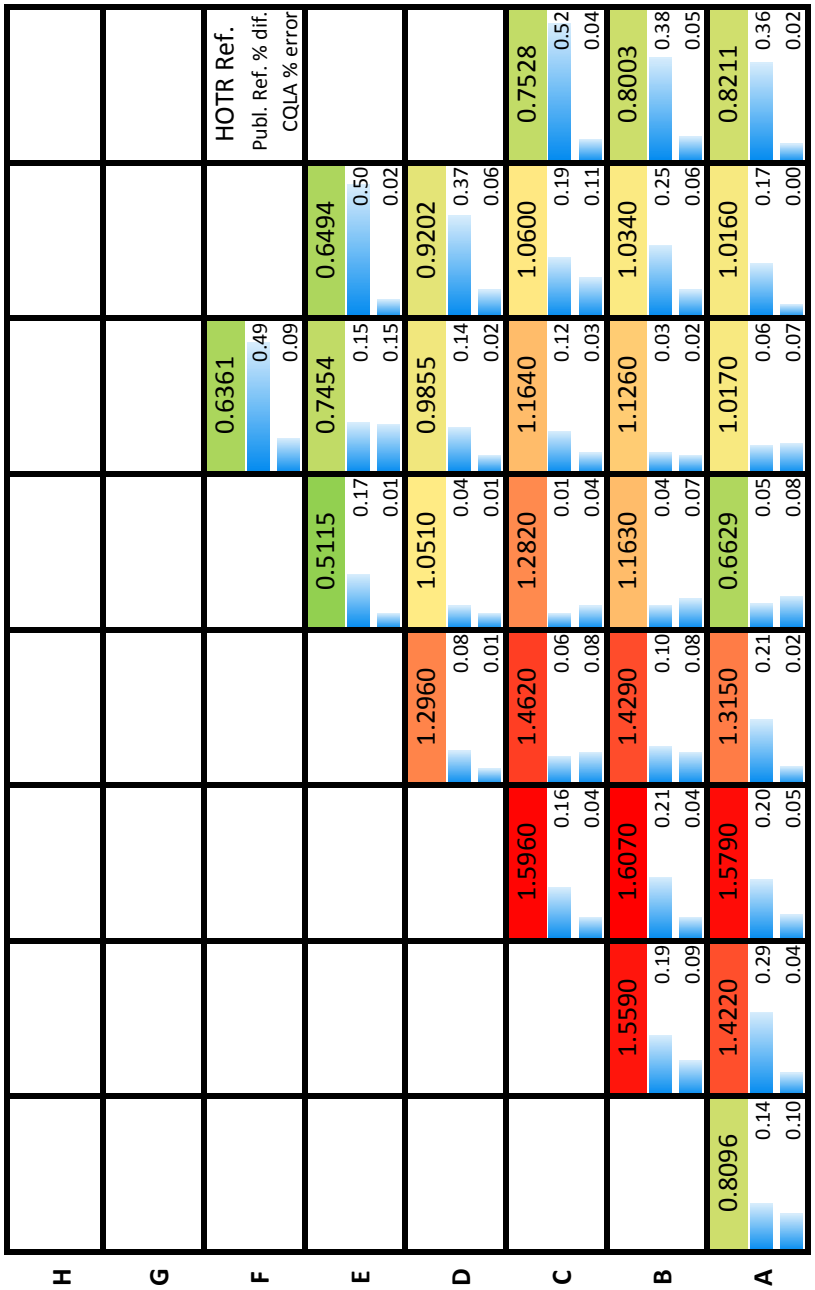

Table B.9: Comparison for IAEA 3D LWR benchmark between published reference, HOTR reference and CQLA power density results for axial layer 14.

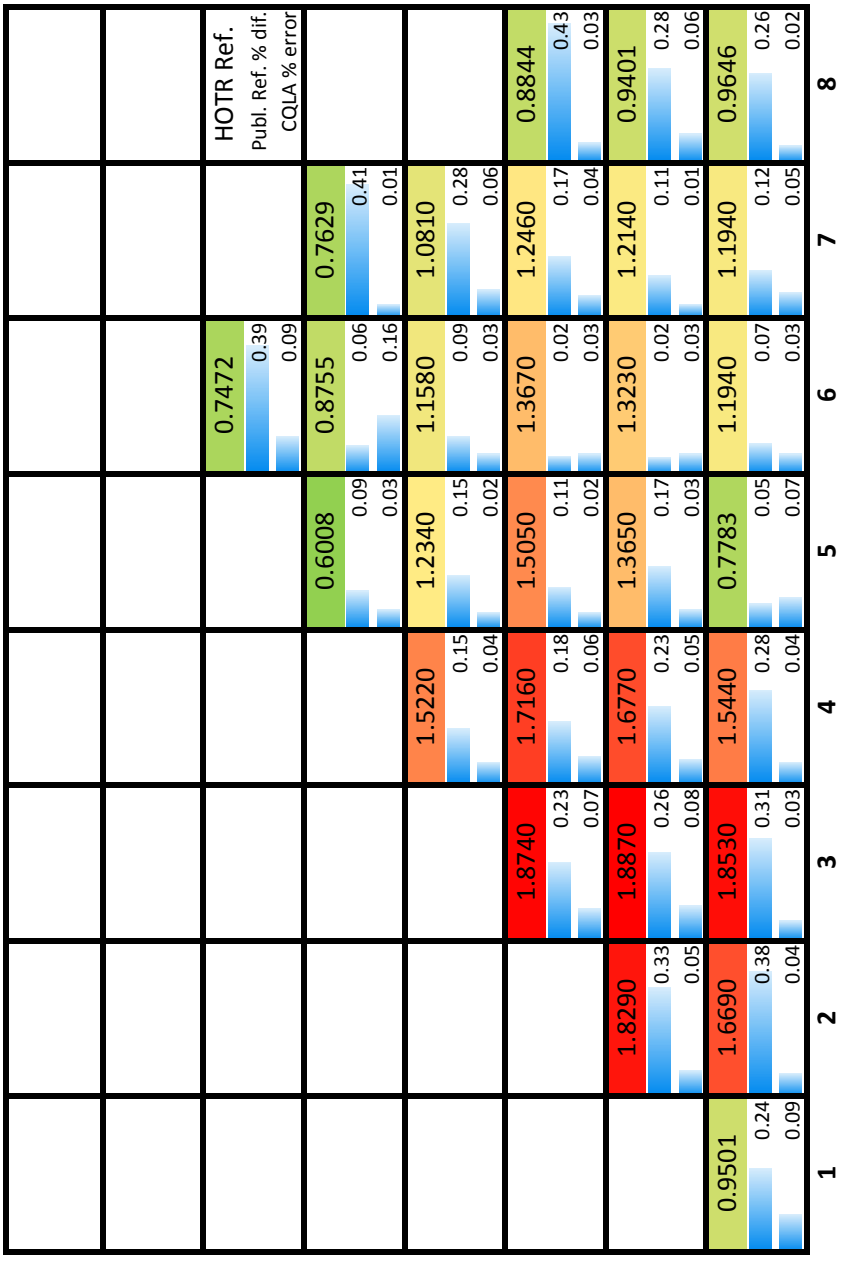

Table B.10: Comparison for IAEA 3D LWR benchmark between published reference, HOTR reference and CQLA power density results for axial layer 13.

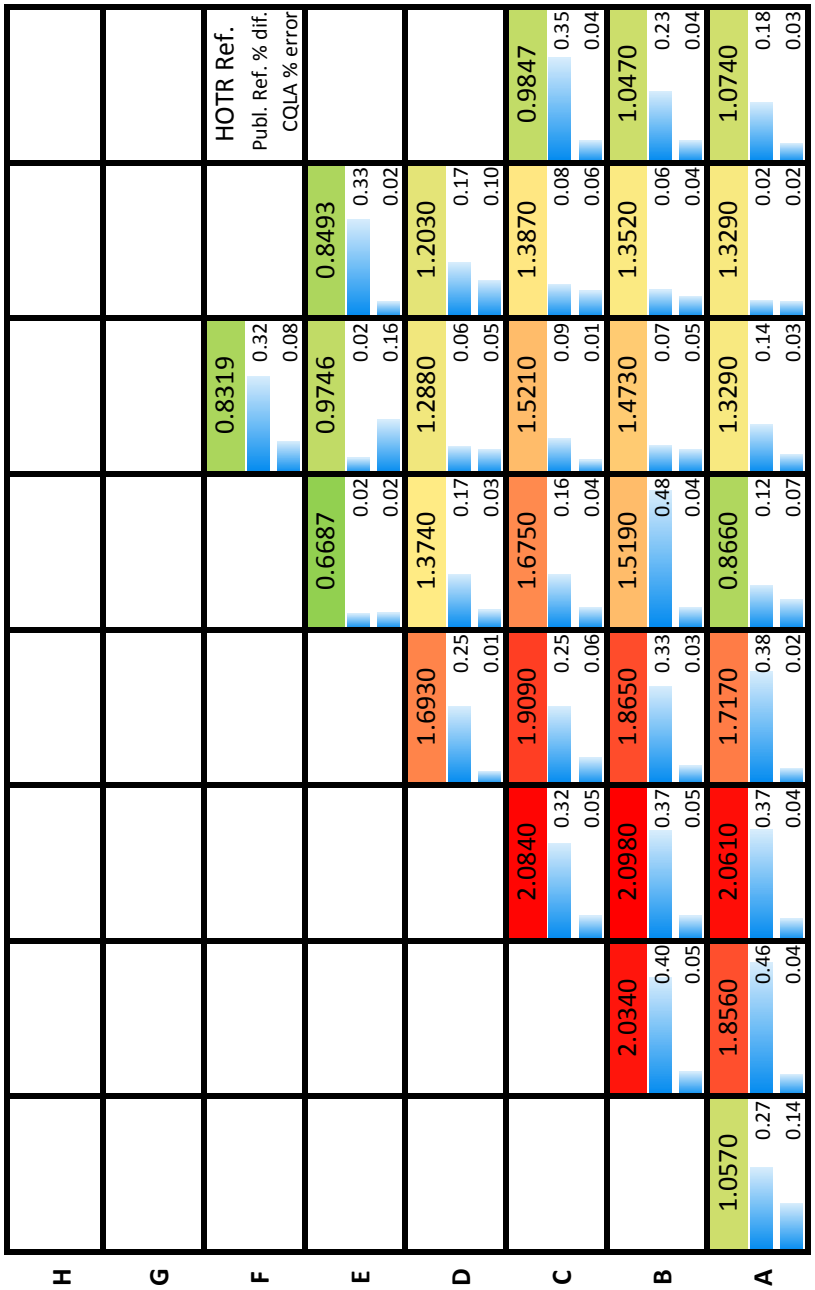

Table B.11: Comparison for IAEA 3D LWR benchmark between published reference, HOTR reference and CQLA power density results for axial layer 12.

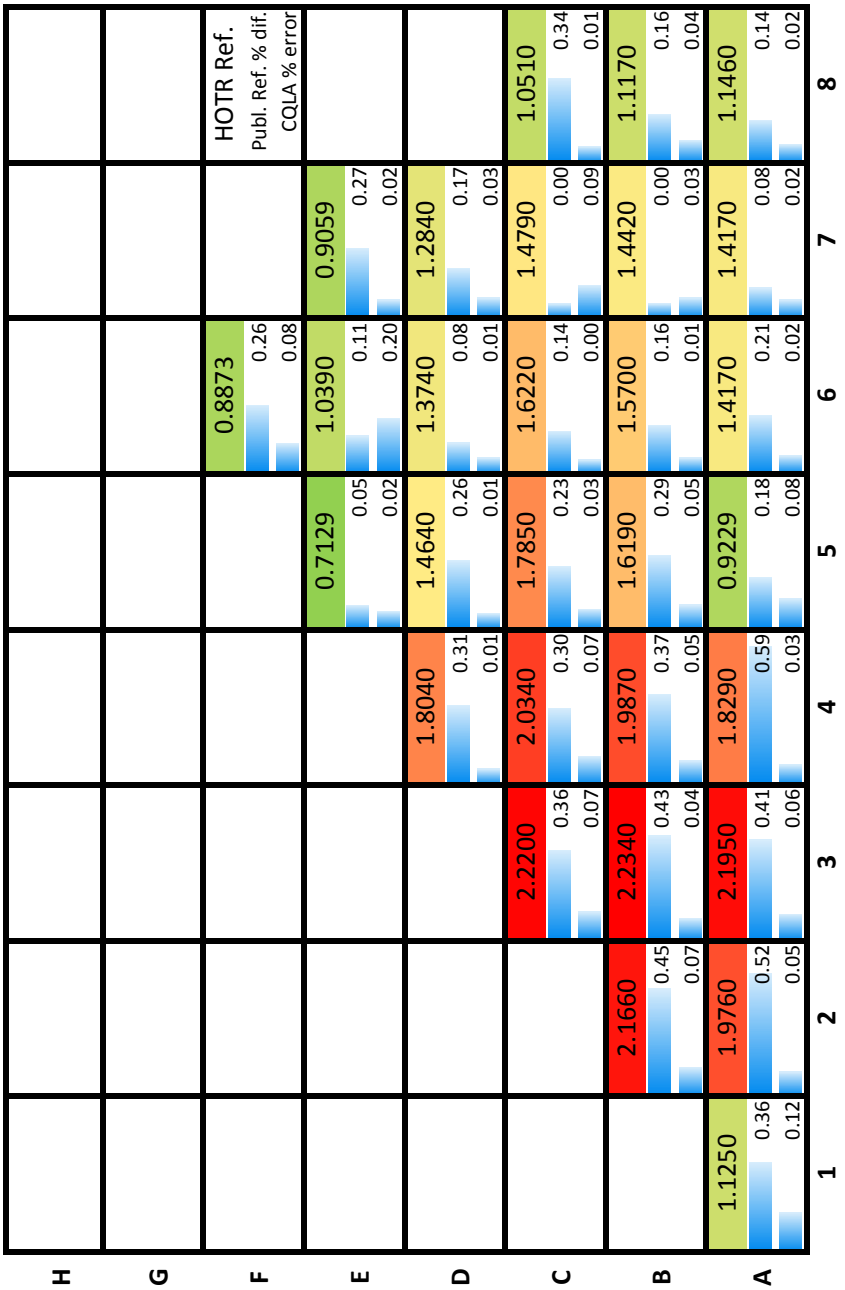

Table B.12: Comparison for IAEA 3D LWR benchmark between published reference, HOTR reference and CQLA power density results for axial layer 11.

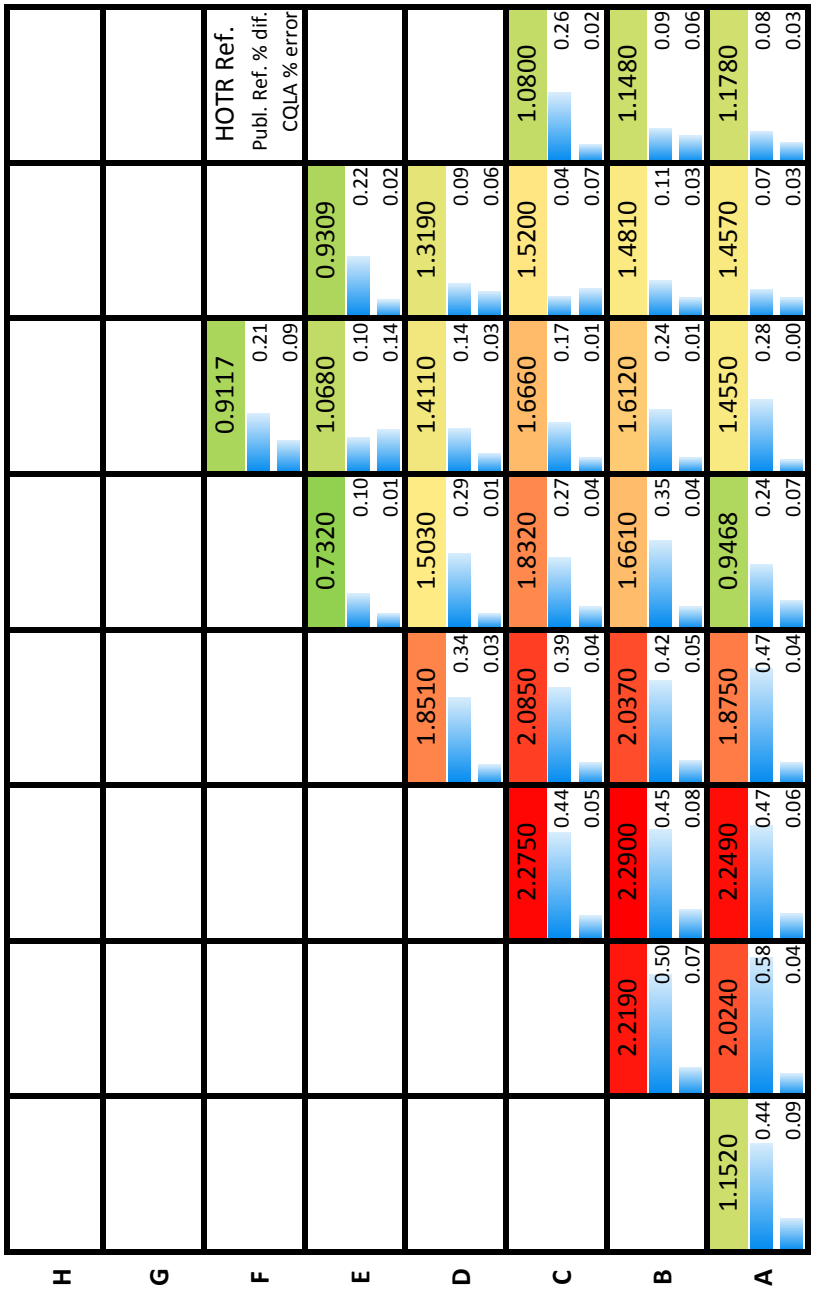

Table B.13: Comparison for IAEA 3D LWR benchmark between published reference, HOTR reference and CQLA power density results for axial layer 10.

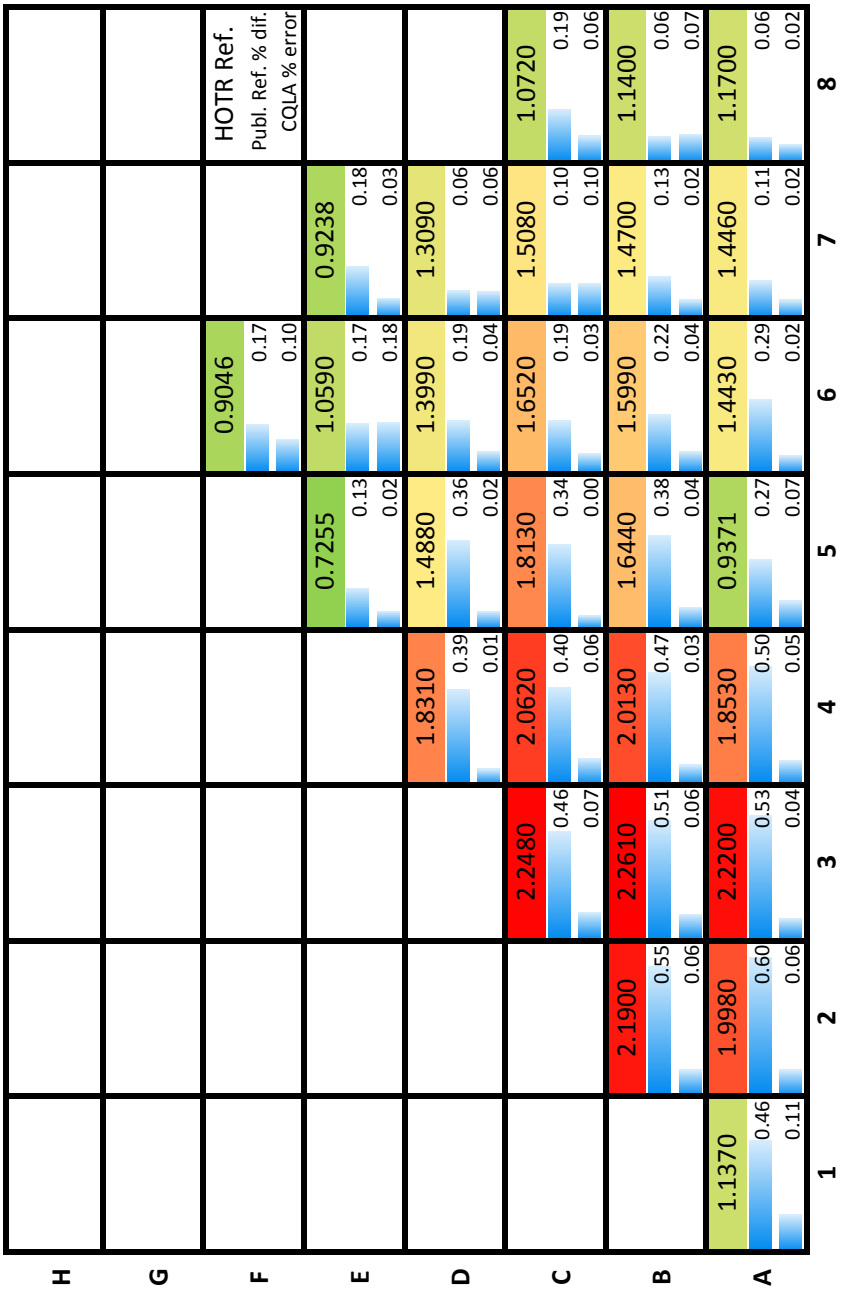

Table B.14: Comparison for IAEA 3D LWR benchmark between published reference, HOTR reference and CQLA power density results for axial layer 9.

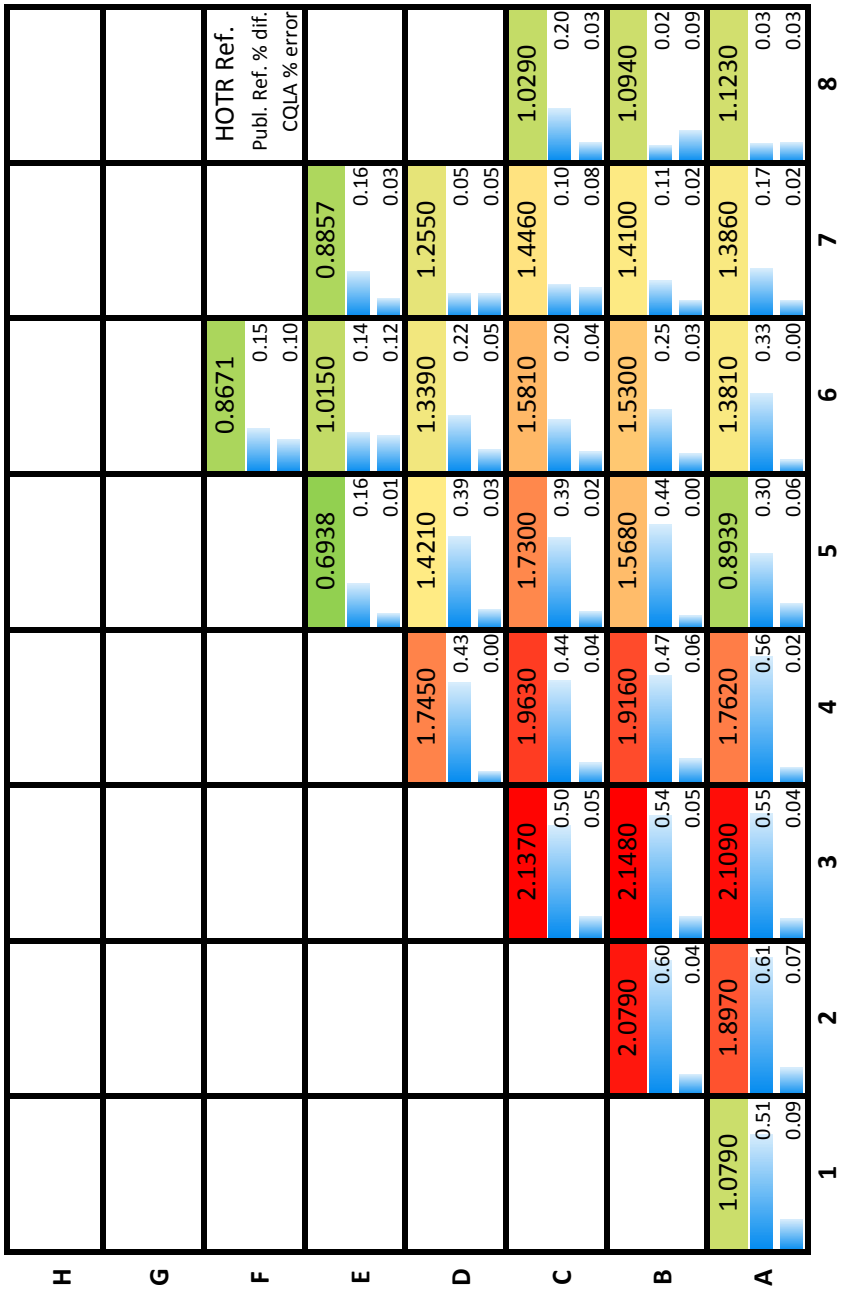

Table B.15: Comparison for IAEA 3D LWR benchmark between published reference, HOTR reference and CQLA power density results for axial layer 8.

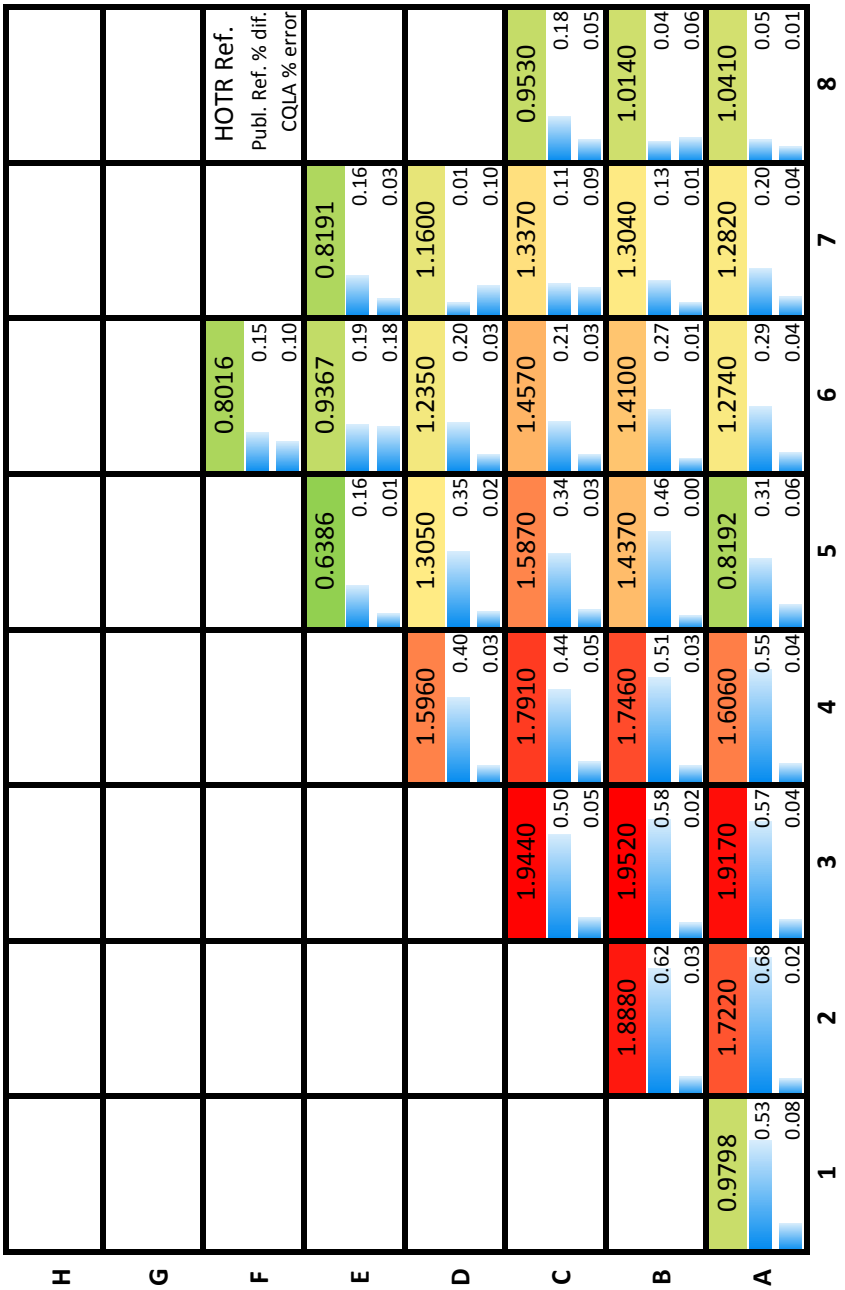

Table B.16: Comparison for IAEA 3D LWR benchmark between published reference, HOTR reference and CQLA power density results for axial layer 7.

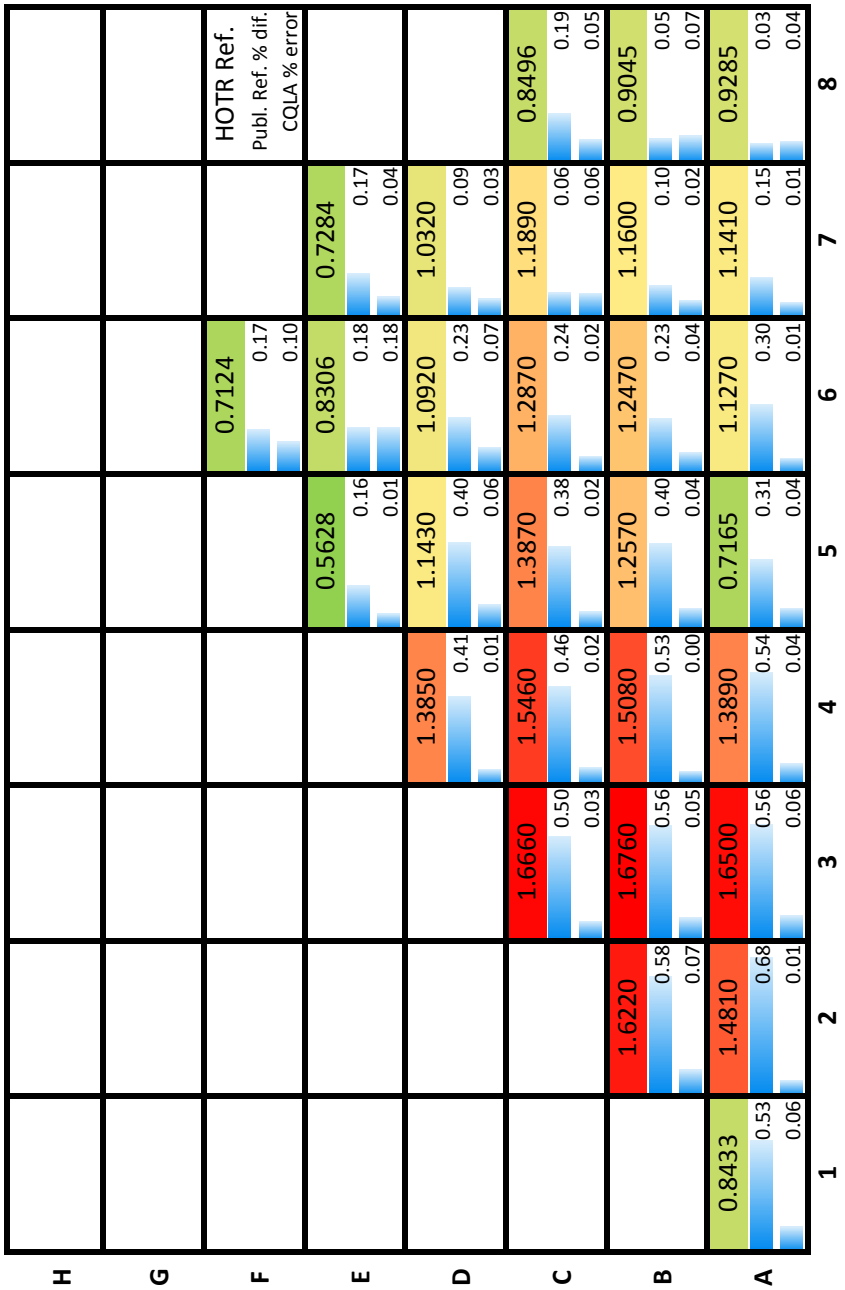

Table B.17: Comparison for IAEA 3D LWR benchmark between published reference, HOTR reference and CQLA power density results for axial layer 6.

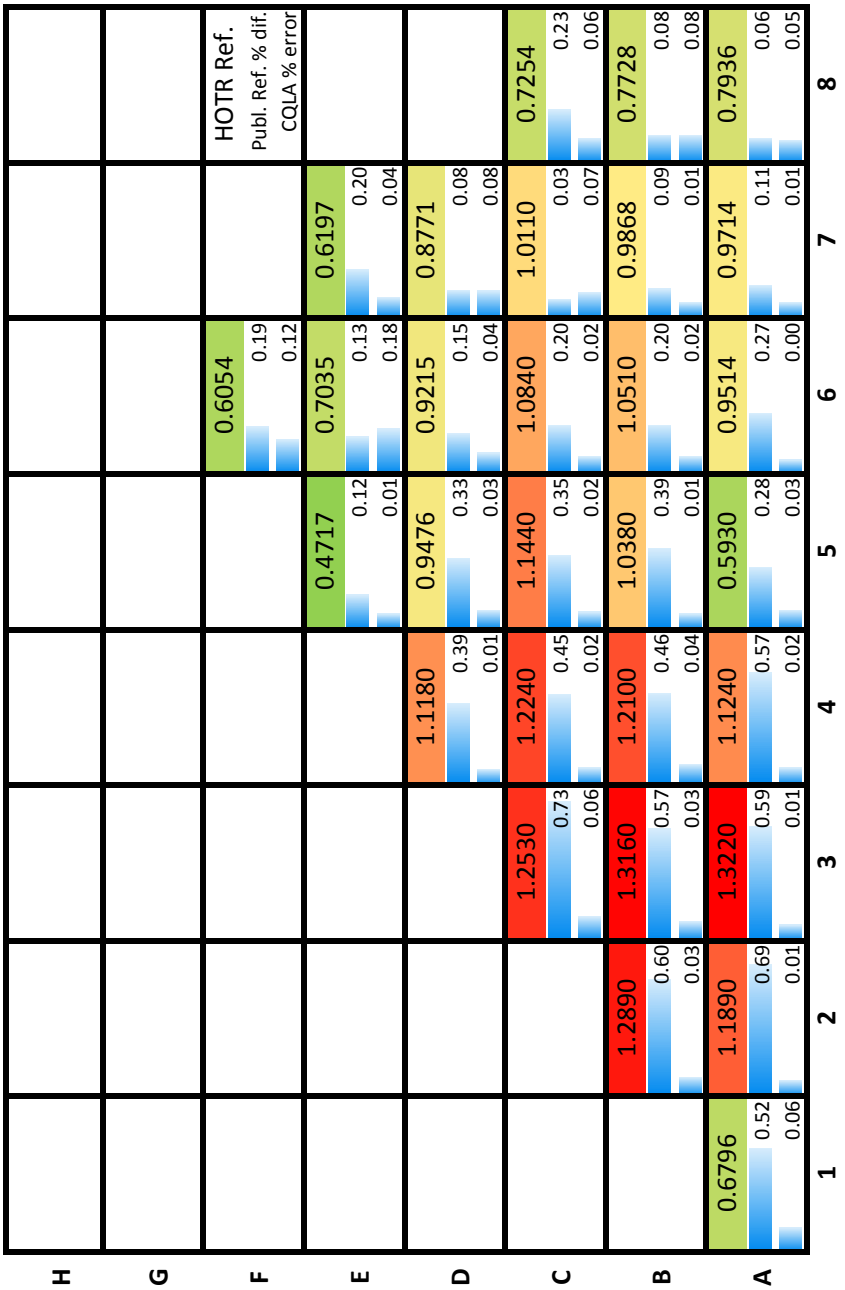

Table B.18: Comparison for IAEA 3D LWR benchmark between published reference, HOTR reference and CQLA power density results for axial layer 5.

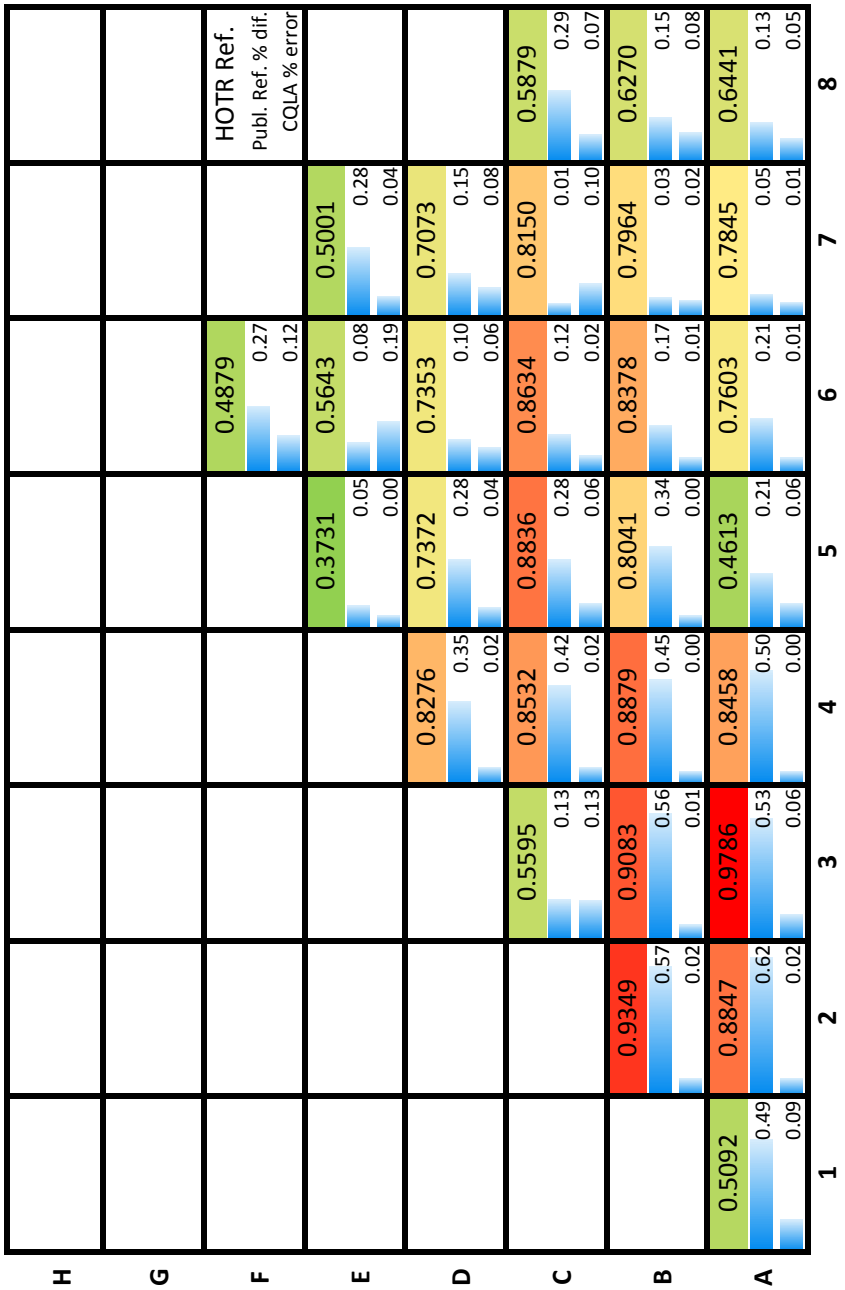

Table B.19: Comparison for IAEA 3D LWR benchmark between published reference, HOTR reference and CQLA power density results for axial layer 4.

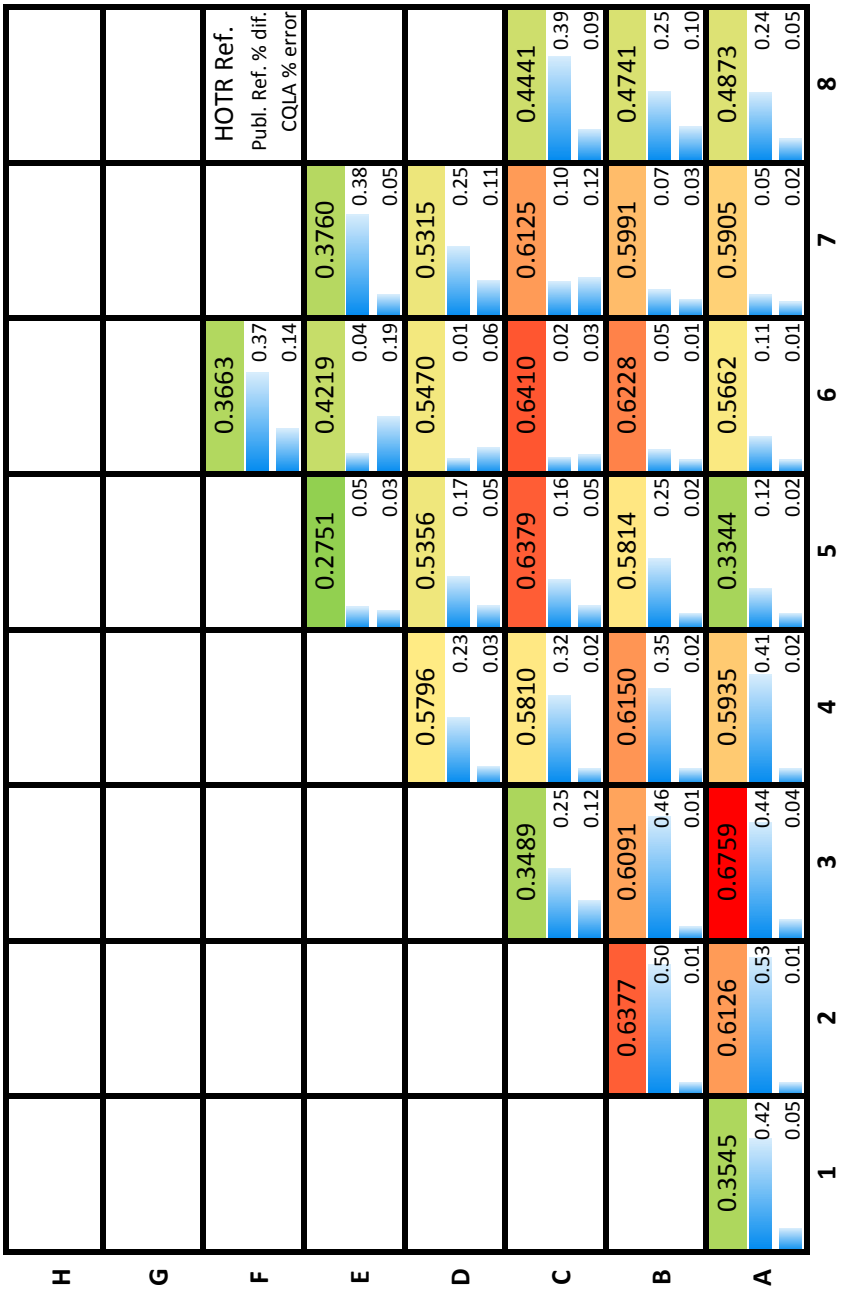

Table B.20: Comparison for IAEA 3D LWR benchmark between published reference, HOTR reference and CQLA power density results for axial layer 3.

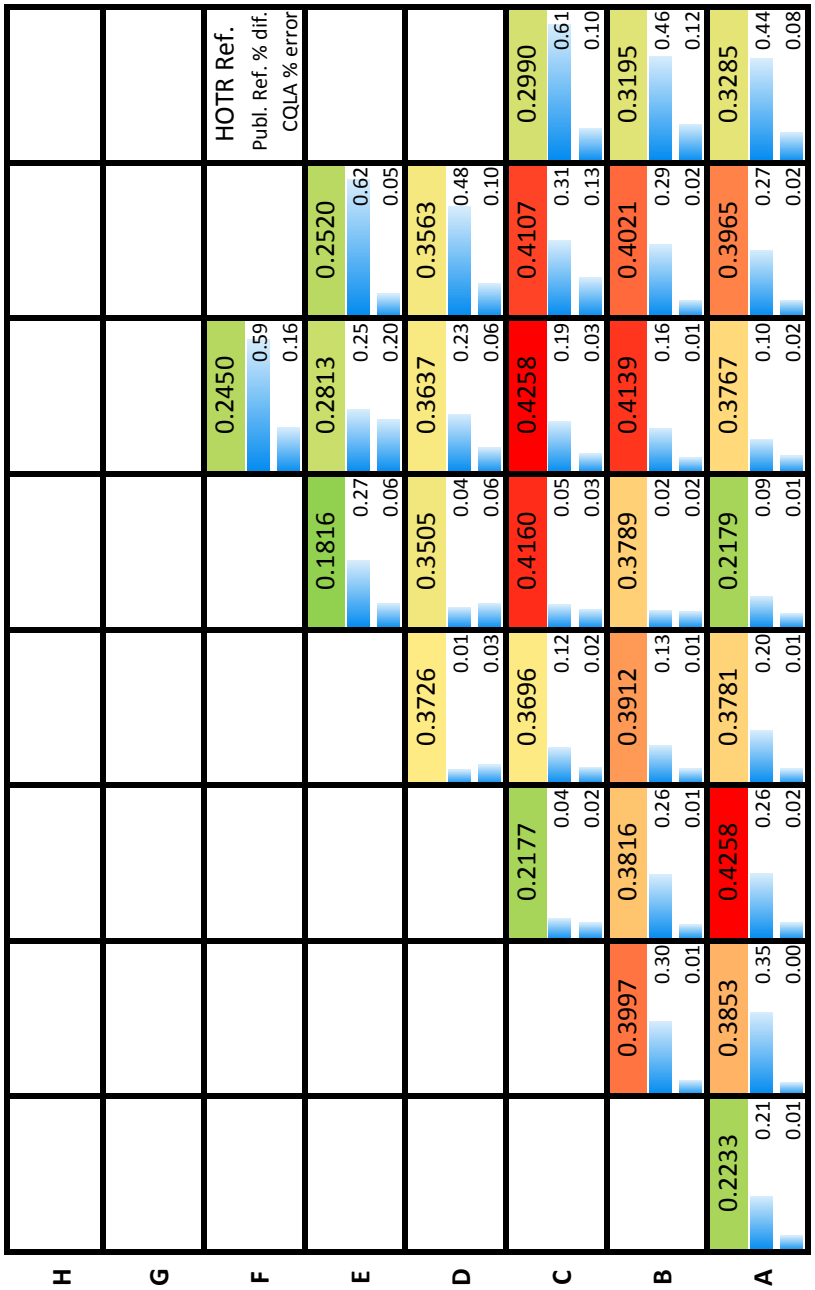

Table B.21: Comparison for IAEA 3D LWR benchmark between published reference, HOTR reference and CQLA power density results for axial layer 2.

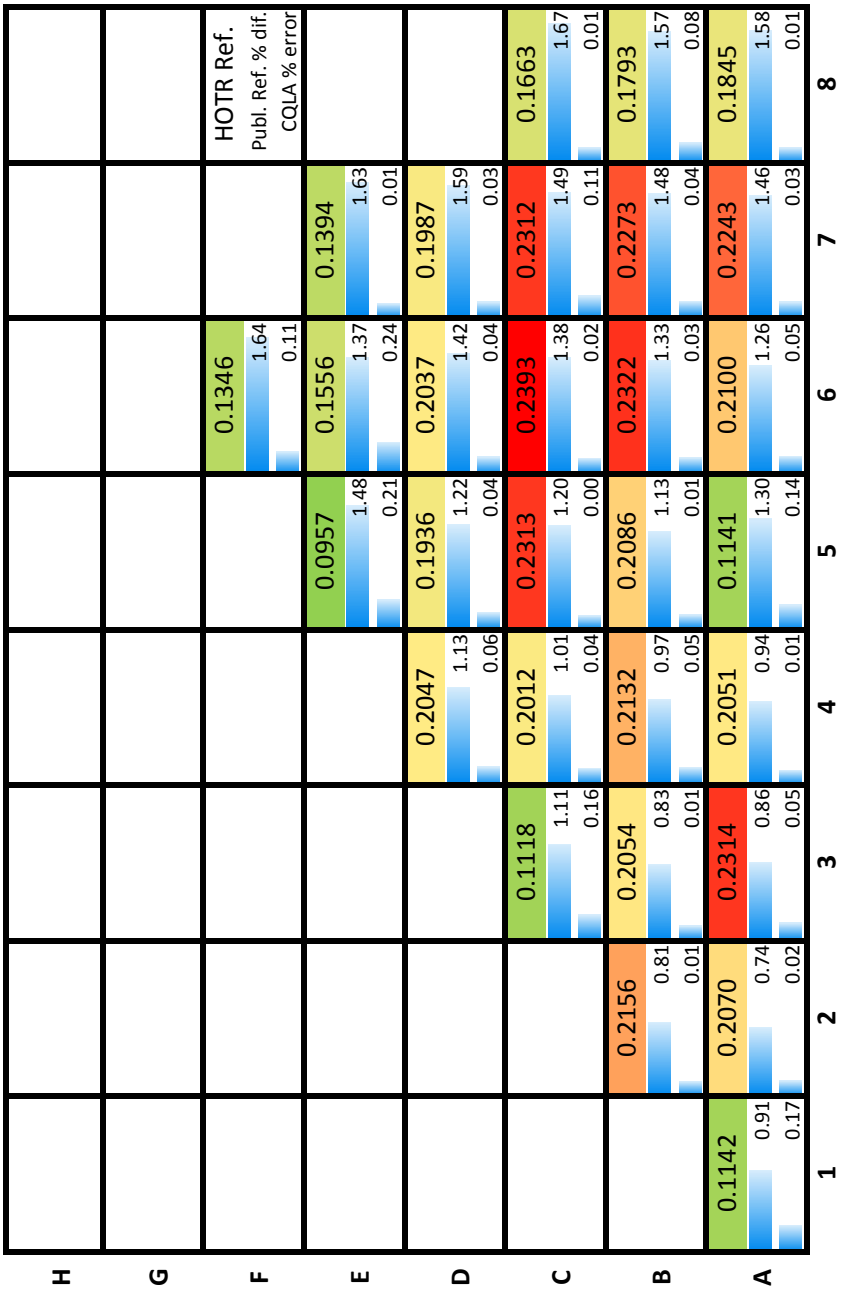

B.4 KOEBERG Benchmark Problem

This section provides some additional results for the KOEBERG 2D 6-group benchmark problem. In particular, six-group flux distributions are given, with SQLA and CQLA errors quantified, in Tables B.22 - B.27. Fluxes are normalized to a core power of 2.75 GW.

Table B.22: Group 1 flux results for the 2D KOEBERG benchmark, with SQLA and CQLA percentage errors indicated in databar format in each cell.

	1	2	3	4	5	6	7	8	9
I	5.275E+03 0.72 0.67	3.875E+03 0.25 0.19	9.622E+02 9.63 0.08						Reference SQLA % error CQLA % error
H	3.660E+04 2.28 0.36	2.883E+04 1.97 0.30	9.665E+03 0.14 0.21	4.214E+03 0.20 0.17	8.961E+02 11.30 0.36				
G	5.103E+04 1.06 0.16	4.990E+04 1.25 0.20	4.322E+04 1.50 0.16	2.921E+04 0.85 0.18	7.313E+03 1.70 0.18	1.000E+03 14.75 0.89			
F	5.850E+04 0.08 0.07	5.581E+04 0.10 0.07	5.293E+04 0.61 0.08	4.678E+04 1.59 0.20	2.941E+04 1.51 0.19	7.149E+03 2.57 0.37	1.000E+03 14.75 0.89		
E	5.907E+04 0.69 0.05	5.986E+04 0.56 0.05	5.528E+04 0.39 0.00	5.021E+04 0.21 0.07	4.146E+04 1.73 0.20	2.941E+04 1.51 0.19	7.313E+03 1.70 0.18	8.961E+02 11.30 0.36	
D	5.765E+04 1.27 0.18	5.777E+04 1.15 0.16	5.895E+04 0.84 0.13	5.411E+04 0.51 0.05	5.021E+04 0.21 0.07	4.678E+04 1.59 0.20	2.921E+04 0.85 0.18	4.214E+03 0.20 0.17	
C	5.470E+04 1.61 0.29	5.601E+04 1.60 0.27	5.712E+04 1.32 0.21	5.895E+04 0.84 0.12	5.528E+04 0.39 0.00	5.293E+04 0.61 0.08	4.322E+04 1.50 0.16	9.665E+03 0.14 0.21	9.622E+02 9.63 0.08
B	5.382E+04 1.95 0.36	5.376E+04 1.80 0.34	5.601E+04 1.60 0.27	5.777E+04 1.15 0.16	5.986E+04 0.56 0.04	5.581E+04 0.10 0.07	4.990E+04 1.25 0.20	2.883E+04 1.97 0.30	3.875E+03 0.25 0.19
A	5.269E+04 1.97 0.39	5.382E+04 1.95 0.36	5.470E+04 1.61 0.29	5.765E+04 1.27 0.18	5.907E+04 0.69 0.05	5.850E+04 0.08 0.07	5.103E+04 1.06 0.16	3.660E+04 2.28 0.36	5.275E+03 0.72 0.67

Table B.23: Group 2 flux results for the 2D KOEBERG benchmark, with SQLA and CQLA percentage errors indicated in databar format in each cell

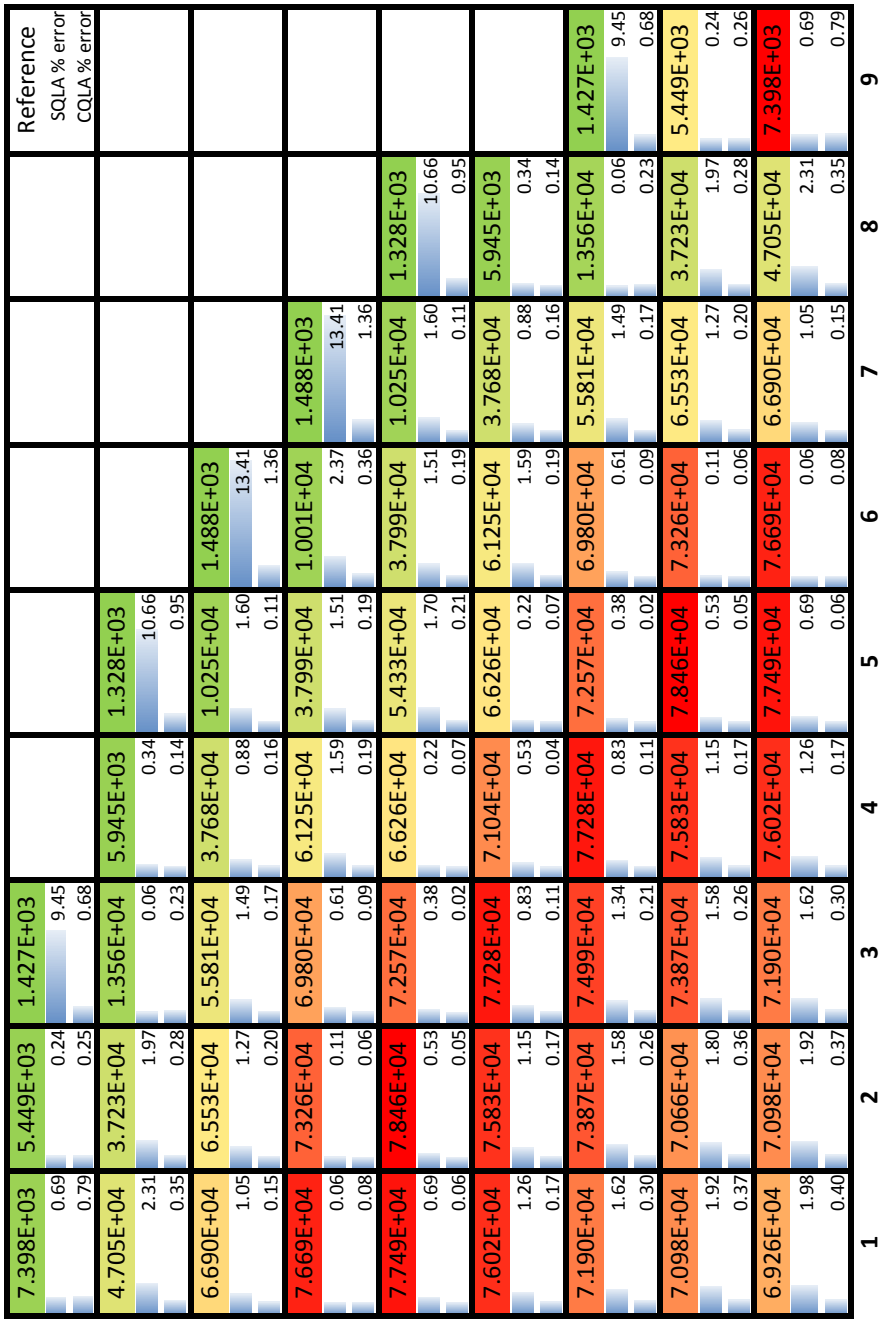

Table B.24: Group 3 flux results for the 2D KOEBERG benchmark, with SQLA and CQLA percentage errors indicated in databar format in each cell

	1	2	3	4	5	6	7	8	9
I	7.398E+03 0.69 0.79	5.449E+03 0.24 0.25	1.427E+03 9.45 0.68						Reference SQLA % error CQLA % error
H	4.705E+04 2.31 0.35	3.723E+04 1.97 0.28	1.356E+04 0.06 0.23	5.945E+03 0.34 0.14	1.328E+03 10.66 0.95				
G	6.690E+04 1.05 0.15	6.553E+04 1.27 0.20	5.581E+04 1.49 0.17	3.768E+04 0.88 0.16	1.025E+04 1.60 0.11	1.488E+03 13.41 1.36			
F	7.669E+04 0.06 0.08	7.326E+04 0.11 0.06	6.980E+04 0.61 0.09	6.125E+04 1.59 0.19	3.799E+04 1.51 0.19	1.001E+04 2.37 0.36	1.488E+03 13.41 1.36		
E	7.749E+04 0.69 0.06	7.846E+04 0.53 0.05	7.257E+04 0.38 0.02	6.626E+04 0.22 0.07	5.433E+04 1.70 0.21	3.799E+04 1.51 0.19	1.025E+04 1.60 0.11	1.328E+03 10.66 0.95	
D	7.602E+04 1.26 0.17	7.583E+04 1.15 0.17	7.728E+04 0.83 0.11	7.104E+04 0.53 0.04	6.626E+04 0.22 0.07	6.125E+04 1.59 0.19	3.768E+04 0.88 0.16	5.945E+03 0.34 0.14	
C	7.190E+04 1.62 0.30	7.387E+04 1.58 0.26	7.499E+04 1.34 0.21	7.728E+04 0.83 0.11	7.257E+04 0.38 0.02	6.980E+04 0.61 0.09	5.581E+04 1.49 0.17	1.356E+04 0.06 0.23	1.427E+03 9.45 0.68
B	7.098E+04 1.92 0.37	7.066E+04 1.80 0.36	7.387E+04 1.58 0.26	7.583E+04 1.15 0.17	7.846E+04 0.53 0.05	7.326E+04 0.11 0.06	6.553E+04 1.27 0.20	3.723E+04 1.97 0.28	5.449E+03 0.24 0.26
A	6.926E+04 1.98 0.40	7.098E+04 1.92 0.37	7.190E+04 1.62 0.30	7.602E+04 1.26 0.17	7.749E+04 0.69 0.06	7.669E+04 0.06 0.08	6.690E+04 1.05 0.15	4.705E+04 2.31 0.35	7.398E+03 0.69 0.79

Table B.25: Group 4 flux results for the 2D KOEBERG benchmark, with SQLA and CQLA percentage errors indicated in databar format in each cell

	1	2	3	4	5	6	7	8	9
I	5.149E+03 0.75 0.84	3.797E+03 0.22 0.29	9.936E+02 9.58 0.92						Reference SQLA % error CQLA % error
H	3.188E+04 2.31 0.36	2.529E+04 1.95 0.30	9.454E+03 0.01 0.24	4.143E+03 0.38 0.11	9.252E+02 10.60 1.21				
G	4.660E+04 1.04 0.15	4.458E+04 1.28 0.20	3.787E+04 1.48 0.18	2.559E+04 0.87 0.18	7.147E+03 1.48 0.11	1.037E+03 13.18 1.55			
F	5.293E+04 0.05 0.08	5.112E+04 0.11 0.06	4.816E+04 0.62 0.09	4.165E+04 1.59 0.19	2.583E+04 1.50 0.20	6.983E+03 2.27 0.31	1.037E+03 13.18 1.55		
E	5.409E+04 0.70 0.05	5.415E+04 0.52 0.04	5.067E+04 0.38 0.02	4.578E+04 0.22 0.08	3.786E+04 1.70 0.19	2.583E+04 1.50 0.20	7.147E+03 1.48 0.11	9.252E+02 10.60 1.20	
D	5.255E+04 1.25 0.16	5.295E+04 1.17 0.16	5.333E+04 0.81 0.12	4.960E+04 0.53 0.04	4.578E+04 0.22 0.08	4.165E+04 1.59 0.19	2.559E+04 0.87 0.18	4.143E+03 0.38 0.11	
C	5.023E+04 1.62 0.31	5.106E+04 1.57 0.26	5.235E+04 1.33 0.22	5.333E+04 0.81 0.12	5.067E+04 0.38 0.02	4.816E+04 0.62 0.09	3.787E+04 1.48 0.18	9.454E+03 0.01 0.25	9.936E+02 9.58 0.91
B	4.907E+04 1.91 0.36	4.937E+04 1.81 0.35	5.106E+04 1.57 0.26	5.295E+04 1.17 0.16	5.415E+04 0.52 0.04	5.112E+04 0.11 0.06	4.458E+04 1.28 0.20	2.529E+04 1.95 0.30	3.797E+03 0.22 0.29
A	4.838E+04 1.98 0.42	4.907E+04 1.91 0.36	5.023E+04 1.62 0.31	5.255E+04 1.25 0.16	5.409E+04 0.70 0.05	5.293E+04 0.05 0.09	4.660E+04 1.04 0.15	3.188E+04 2.31 0.36	5.149E+03 0.75 0.84

Table B.26: Group 5 flux results for the 2D KOEBERG benchmark, with SQLA and CQLA percentage errors indicated in databar format in each cell

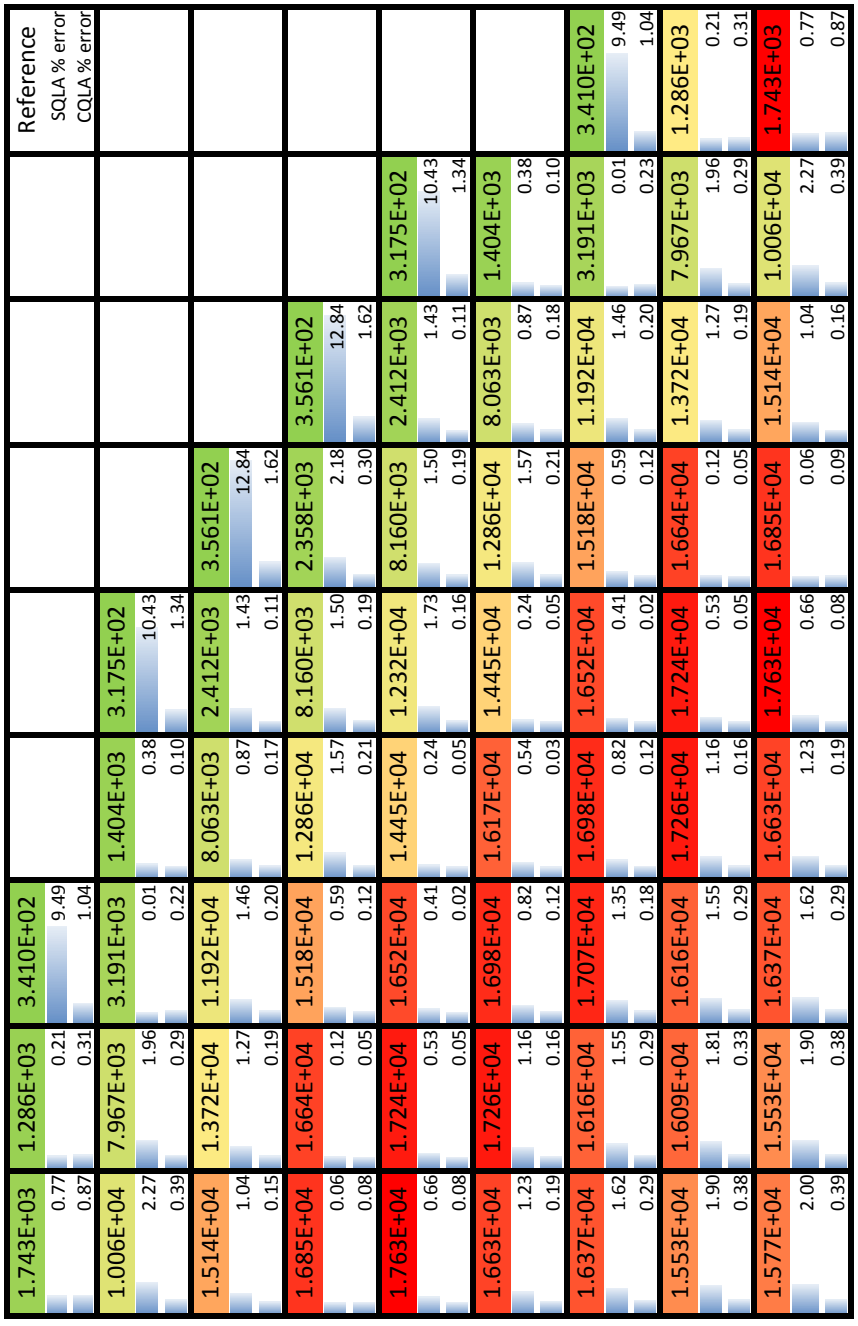

Table B.27: Group 6 flux results for the 2D KOEBERG benchmark, with SQLA and CQLA percentage errors indicated in databar format in each cell.

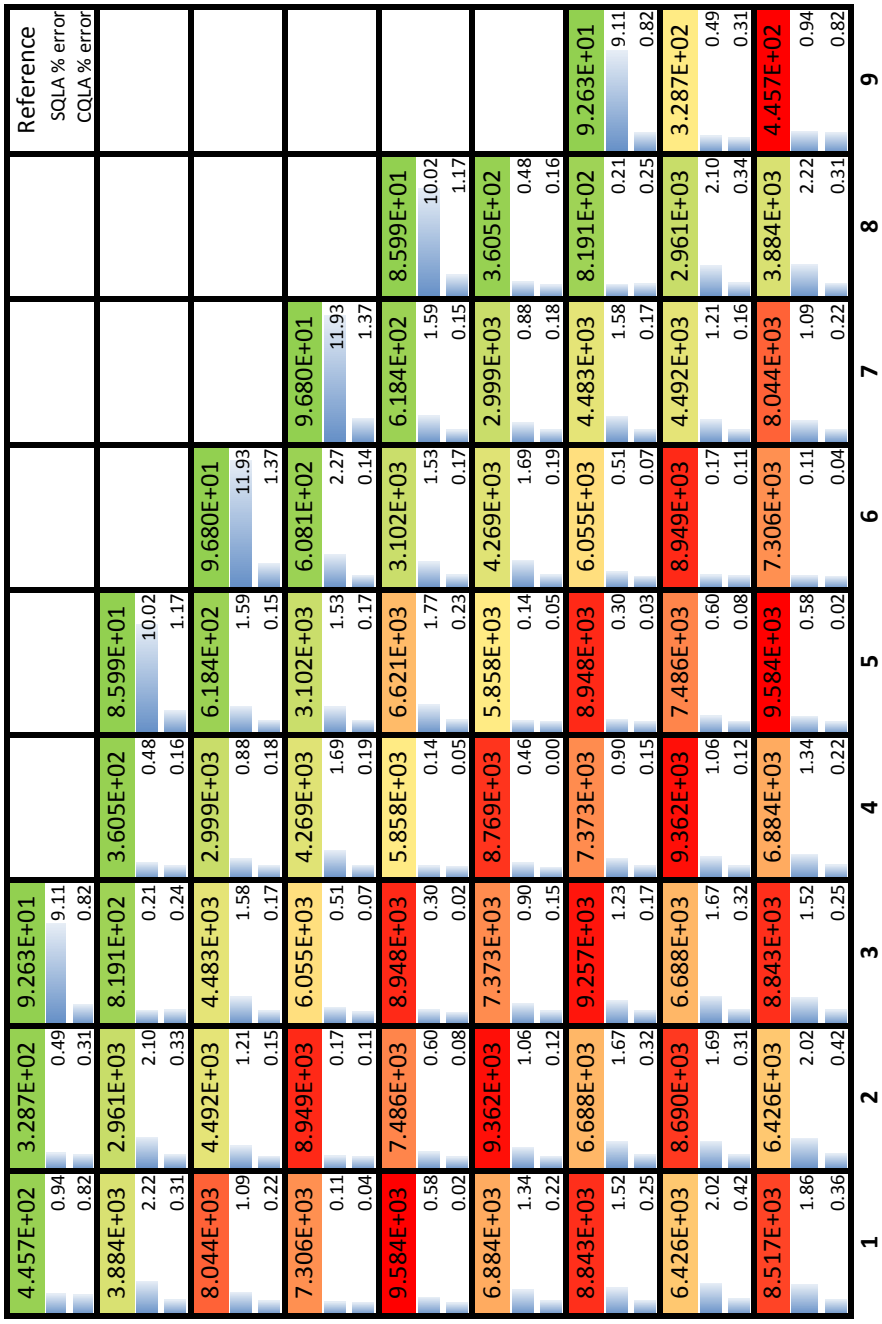

Finally, Figure B.1 represents a SQLA error distribution for the KOEBERG benchmark problem.

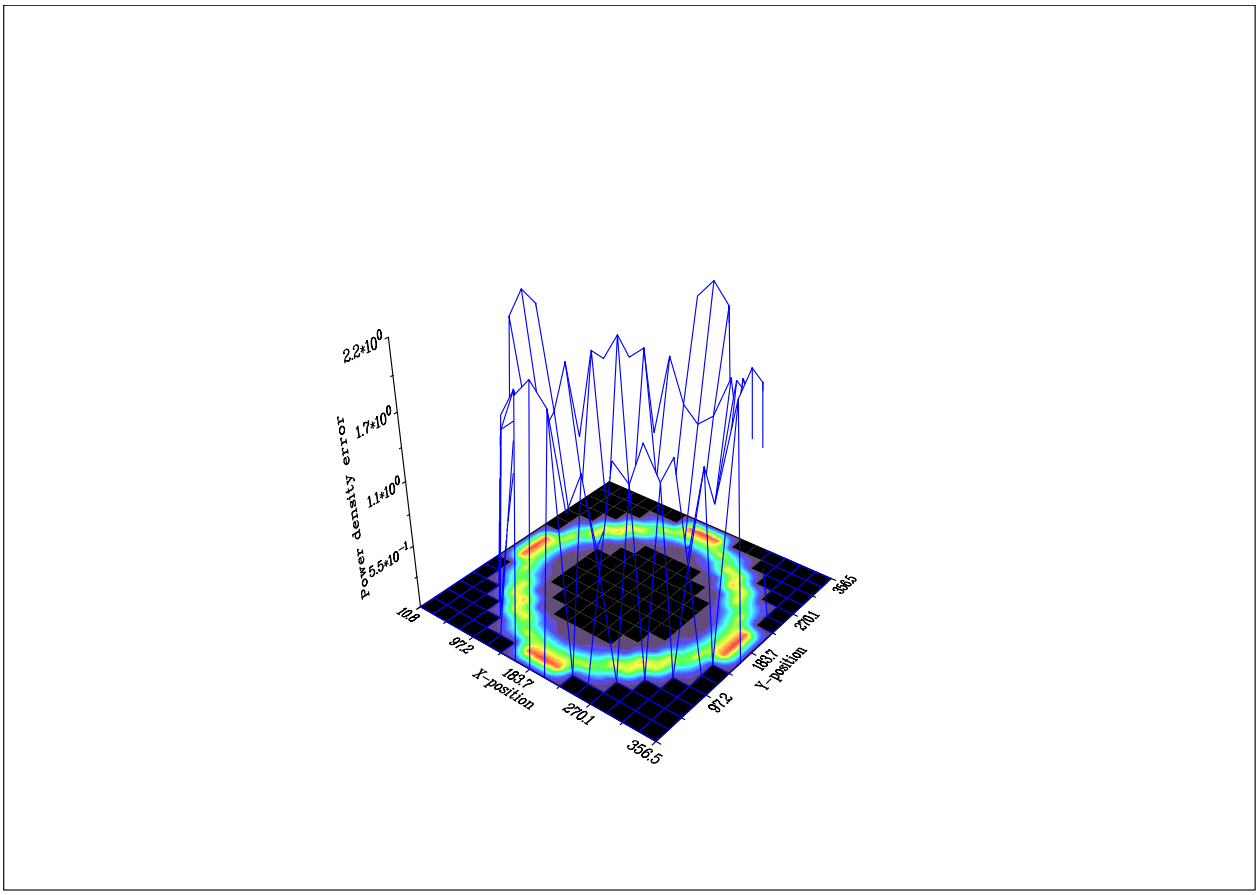

Figure B.1: SQLA power density error distribution for the KOEBERG benchmark problem.

B.5 SAFARI-1 Benchmark Problem

The SAFARI-1 benchmark problem represents a realistic 3D 6-group snapshot of the SAFARI-1 reactor which operates at Necsa, in South Africa. The assembly-averaged power density reference solution, with percentage errors from the SQLA and CQLA solutions, is presented in Table

Table B.28: Reference assembly-averaged power density distribution for the 3D 6-group SAFARI-1 benchmark, with SQLA and CQLA percentage errors indicated with in databar format in each cell.

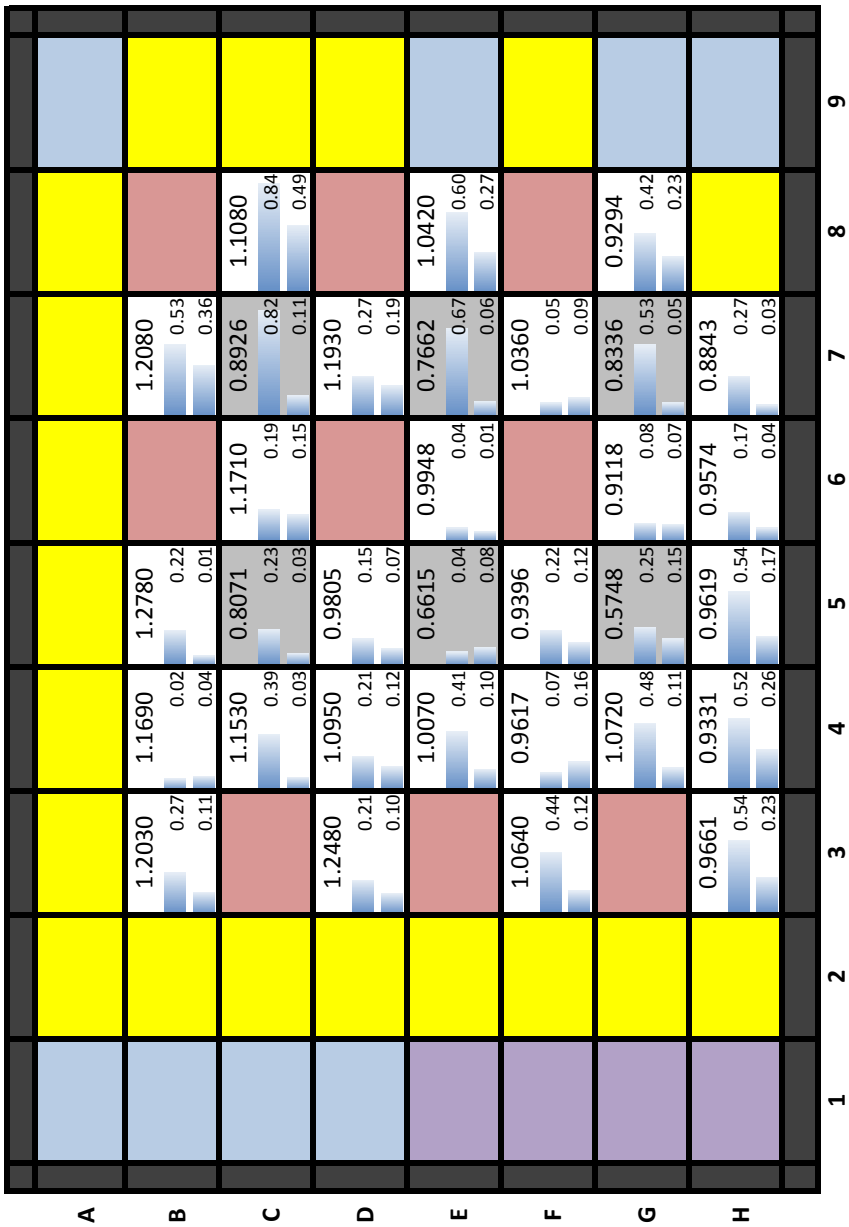

Appendix C

Recurrence relationships for Legendre moments of hyperbolic functions

We first derive recurrence relationship for integrals of exponential-polynomial form.

$$I_l = \int_{-1}^{1} e^{aw} P_l(w) dw = -\frac{2l-1}{a} I_{l-1} + I_{l-2},\ a \neq 0 \tag{C.1}$$

with

$$I_0 = \frac{2}{a}\sinh(a)\ ,\ I_1 = \frac{2}{a}(\cosh(a) - \frac{\sinh(a)}{a}),\ a \neq 0$$

Utilizing the relationships

$$\cosh(\beta) = \frac{1}{2}\left(e^{\beta} + e^{-\beta}\right) \text{ and } \sinh(\beta) = \frac{1}{2}\left(e^{\beta} - e^{-\beta}\right)$$

moments of one-dimensional flux are separately calculated in their cosh, sinh and particular solution components. Let us define firstly the hyperbolic cosine moments, which exist only for l even:

$$f_l^{cos} = \int_{-1}^{1} \cosh(|\beta^{nm}|\, w) P_l(w) dw = \frac{1}{2}\left(-\frac{2l-1}{|\beta^{nm}|} I_{l-1}^{cos,+} + I_{l-2}^{cos,+} + \frac{2l-1}{|\beta^{nm}|} I_{l-1}^{cos,-} + I_{l-2}^{cos,-}\right) \tag{C.2}$$

$$I_0^{cos,+} = \frac{2}{|\beta^{nm}|}\sinh(|\beta^{nm}|)\ ,\ I_1^{cos,+} = \frac{2}{|\beta^{nm}|}(\cosh(|\beta^{nm}|) - \frac{\sinh(|\beta^{nm}|)}{|\beta^{nm}|})$$

$$I_0^{cos,-} = \frac{2}{\overline{\beta_n^{nm}}}\sinh(\overline{\beta_n^{nm}})\ ,\ I_1^{cos,-} = \frac{-2}{\overline{\beta_n^{nm}}}(\cosh(\overline{\beta_n^{nm}}) - \frac{\sinh(|\beta^{nm}|)}{|\beta^{nm}|})$$

$$I_l^{cos,+} = -\frac{2l-1}{|\beta^{nm}|} I_{l-1}^{cos,+} + I_{l-2}^{cos,+}$$

$$I_l^{cos,-} = \frac{2l-1}{|\beta^{nm}|} I_{l-1}^{cos,+} + I_{l-2}^{cos,+}$$

$$f_0^{cos} = \frac{1}{2}\left(I_0^{cos,+} + I_0^{cos,-}\right)$$

$$f_1^{cos} = \frac{1}{2}\left(I_1^{cos,+} + I_1^{cos,-}\right)$$

for

$$l = 0, 2, 4, ...$$

Similarly define :

$$f_l^{sin} = \int_{-1}^{1} \sinh(|\beta^{nm}|\, w) P_l(w) dw = \frac{1}{2}\left(-\frac{2l-1}{|\beta^{nm}|} I_{l-1}^{sin,+} + I_{l-2}^{sin,+} - \frac{2l-1}{|\beta^{nm}|} I_{l-1}^{sin,-} - I_{l-2}^{sin,-}\right) \tag{C.3}$$

$$I_0^{sin,+} = \frac{2}{|\beta^{nm}|}\sinh(|\beta^{nm}|) \ , \ I_1^{sin,+} = \frac{2}{|\beta^{nm}|}(\cosh(|\beta^{nm}|) - \frac{\sinh(|\beta^{nm}|)}{|\beta^{nm}|})$$

$$I_0^{sin,-} = \frac{2}{|\beta^{nm}|}\sinh(|\beta^{nm}|) \ , \ I_1^{sin,-} = \frac{-2}{|\beta^{nm}|}(\cosh(|\beta^{nm}|) - \frac{\sinh(|\beta^{nm}|)}{|\beta^{nm}|})$$

$$I_l^{sin,+} = -\frac{2l-1}{|\beta^{nm}|} I_{l-1}^{sin,+} + I_{l-2}^{sin,+}$$

$$I_l^{sin,-} = \frac{2l-1}{|\beta^{nm}|} I_{l-1}^{sin,-} + I_{l-2}^{sin,-}$$

$$f_0^{sin} = \frac{1}{2}\left(I_0^{sin,+} - I_0^{sin,-}\right)$$

$$f_1^{sin} = \frac{1}{2}\left(I_1^{sin,+} - I_1^{cos,-}\right)$$

for

$$l = 1, 3, 5, ...$$